mice were obtained from Jackson Laboratory (Bar Harbor, ME). DKO mice were generated by mating LKO mice with AKO mice. After genotyping by polymerase chain reaction analysis, littermates from the F2 generation of this crossbreed were used to establish DKO mating, and the resulting progeny was used in our study. All animals were of pure (9-generation backcross) C57BL/6 genetic background. Male mice were fed a normal chow diet until 8 weeks of age, after which they received a high-fat diet containing 30% fat (Oriental Yeast Co., Tokyo, Japan) for 20 weeks. Mice were maintained in an air-conditioned room (25 °C; humidity 50%) with a 12 h light and dark cycle. Animals had free access to diet and drinking water but were not fed overnight prior to the experiments.

During the high-fat feeding, body weight and systolic blood pressure (BP) were measured every 4 weeks. Systolic BP was examined by tail-cuff plethysmography (BP98-A, Softron Co., Tokyo, Japan) on conscious restrained mice. Each measurement was performed five times, and values were averaged and recorded. Food intake was monitored daily for a period of 7 days in single-housed mice. After a week of acclimatization to the new environment, the amount of diet ingested was calculated as the difference between the weight of the food remaining in the food bin and the amount of pre-weighed food added the day before. Serum levels of cholesterols, triglyceride, creatinine and adiponectin were determined using blood samples collected from mice at 12 weeks after starting the high-fat diet.

Intraperitoneal glucose tolerance tests were performed in mice fasted for 16 h. Blood was collected before and after intraperitoneal injection of glucose (1 g/kg) at 15, 30, 60, 90 and 120 min. Intraperitoneal insulin tolerance test was performed after mice were fasted for 5 h. Blood glucose levels were measured prior to the injection of insulin (1.0 U/kg; Novolin®, Novo Nordisk Pharmaceuticals, Inc., Princeton, NJ) and at 15, 30, 60, 90 and 120 min after injection.

Magnetic resonance imaging (MRI) studies. In vivo MRI scanning was performed using a 0.3-T open MRI (AIRIS II, Hitachi Medico., Tokyo, Japan) to determine body fat distribution. Mice were anesthetized with pentobarbital (50 μg/g) and placed in a coil. T1-weighted SE sequence (TR/TE = 450/14 ms; FOV 85 mm; matrix 512 × 512; slice thickness 2 mm) was used to acquire 14 transverse slices. To evaluate the volumes of visceral and subcutaneous adipose tissue compartments, digital images were captured and hyper-intense fat was manually segmented and areas calculated as pixels using NIH Image J software (version 1.6.0, National Institute of Health, ML). The average values obtained from six consecutive slices between the middle of the right kidney to urinary bladder were defined as the fat tissue volume.

Measurements of adipocyte sizes. To determine adipocyte sizes of visceral and subcutaneous fat, the cross-sectional area of adipocytes was measured on paraffin-embedded hematoxylin–eosin-stained sections as previously described [15]. After converting the image of adipose tissue under the microscope to a binary image, each adipocyte from five randomly chosen fields (approximately 100 cells per mouse) was manually segmented and the areas calculated as pixels using NIH Image J software.

En face evaluation of atherosclerotic lesions. After the mice were fed with a high-fat diet for 20 weeks, they were anesthetized with pentobarbital and perfused with Krebs-Ringer solution, and the aorta was dissected from the aortic valve to the iliac bifurcation under a light microscope. The whole aorta was fixed in 10% formaldehyde for over 24 h, and opened longitudinally and pinned onto a black wax surface. To identify lipid-rich intraluminal lesions, the aorta was stained for 30 min in a saturated Oil-Red-O solution at room temperature. Digital images of the aortic lumen en face under the microscope were captured and saved on a computer and the index of atherosclerotic formation ([total lesion area/total surface area] × 100%) in the aortic arch was calculated for each aorta using NIH Image J software.

Histological examination of the aortic root. The aortic root was dissected and placed in 10% formaldehyde for 24 h and then transferred to 10–30% sucrose solution for 3 days. After embedding in OCT compound (Tissue-Tek), 10-μm-thick sections of the aortic roots were cut using a cryostat at −20 °C. Some of the sections were stained for 15 min in a saturated Oil-Red-O solution at room temperature and counterstained with hematoxylin. For quantitative estimation of the plaque contents, we analyzed the Oil-Red-O-stained areas as previously described [16] using NIH Image J software. The remaining sections were used for immunohistochemical analysis using the following antibodies: monoclonal anti-CD68 (AbD Serotec, Kidlington, UK), polyclonal anti-macrophage chemoattractant protein-1 (MCP-1) (sc-1785, Santa-Cruz, CA) and polyclonal anti-IL-1β (sc-7884; Santa-Cruz). After blocking endogenous peroxidase with 3% H_2O_2 in methanol for 30 min, serial 5-μm-thick cryosections of the aortic root were incubated with each antibody (1:100) overnight at 4 °C. The sections were treated with secondary biotinylated antibodies and incubated with streptavidin labeled with horseradish peroxidase using a Histofine SAB-PO Kit (Nichirei Co., Tokyo, Japan). The sections were then counterstained with hematoxylin. Under the microscope, percentages of stained cells from five randomly chosen fields were manually calculated.

Statistical analysis. Differences between groups were determined by two-tailed Student's *t*-test or one-way analysis of variance (ANOVA). When a significant difference was observed in ANOVA, the difference between two groups was analyzed by post hoc analysis. $P < 0.05$ was considered to be significant.

Results

Effect of l-pgds deficiency on phenotype

After the mice were fed a high-fat diet for 12 weeks from 8-weeks-old, the body weight of *l-pgds*-deficient (LKO and DKO) mice was significantly increased compared with the respective control (WT and AKO) mice (Table 1). When we compared diet consumption among the mice, food intake was significantly lower in *apo E*-deficient (AKO and DKO) mice compared with the WT and LKO mice, whereas *l-pgds* deficiency did not affect food intake. The body weight of *apo E*-deficient mice was also relatively lower but not statistically significant. Although the levels of systolic BP were not influenced by genotype, the serum levels of total cholesterol, LDL-cholesterol and triglyceride were significantly higher in *apo E*-deficient (AKO and DKO) mice. The *l-pgds* deficiency tended to increase total and LDL-cholesterol and triglyceride, although this was not statistically significant. HDL-cholesterol was relatively lower in DKO mice compared with AKO mice, but no difference was observed between WT and LKO mice. Because a recent report [17] showed that *l-pgds* KO mice become glucose intolerant and insulin resistant, we performed an intraperitoneal glucose tolerance test and insulin tolerance test. However, *l-pgds* deficiency did not significantly affect glucose or insulin tolerance (data not shown). Similarly, *l-pgds* deficiency did not affect the serum level of adiponectin, which is an insulin-sensitizing hormone that is exclusively expressed in adipose tissues (Table 1).

Next, to compare the fat tissue volume between *l-pgds*-deficient mice and control mice, we performed abdominal MRI using an open MRI scanner. As shown in Fig. 1A, we evaluated the volumes of visceral and subcutaneous adipose tissue compartments from six consecutive slices between the center of the right kidney (left) and the urinary bladder (right). Significant increases in volume of subcutaneous and visceral fat tissues were observed in MRI images in *l-pgds*-deficient (LKO and DKO) mice (Fig. 1B). These results

Table 1
Characteristics of mice (at 20-week-old).

	WT	LKO	AKO	DKO
Number	8	8	6	6
Food intake (g/week)	31 (1.0)	30 (1.0)	26 (1.5)*	22 (0.7)*
Weight (g)	37.1 (1.4)	46.7 (1.9)*	34.5 (1.2)	40.7 (1.0)†
Systolic blood pressure (mm Hg)	104.6 (5.1)	103.6 (7.3)	101.6 (5.0)	111.4 (7.0)
Total cholesterol (mg/dL)	153.2 (17.2)	189.2 (50.6)	427.5 (77.7)*	485.7(25.1)*
LDL-cholesterol (mg/dL)	18.0 (3.0)	24.5 (7.5)	124.0 (23.1)*	139.0 (3.6)*
HDL-cholesterol (mg/dL)	61.6 (10.0)	63.3 (8.1)	45.5 (10.1)	38.0 (3.8)
Triglyceride (mg/dL)	12.3 (1.6)	12.7 (2.2)	48.3 (17.0)*	68.0 (12.4)*
Adiponectin (mg/mL)	9.6 (2.4)	10.1 (2.6)	17.3 (1.8)*	18.4 (3.3)

WT, wild type mice; LKO, *l-pgds* knockout mice; AKO, *apo E* knockout mice; DKO, *l-pgds/apo E* double knockout mice; LDL, low density lipoprotein; HDL, high density lipoprotein.
Data represent means (SE).
* $P < 0.05$ vs WT.
† $P < 0.05$ vs AKO.

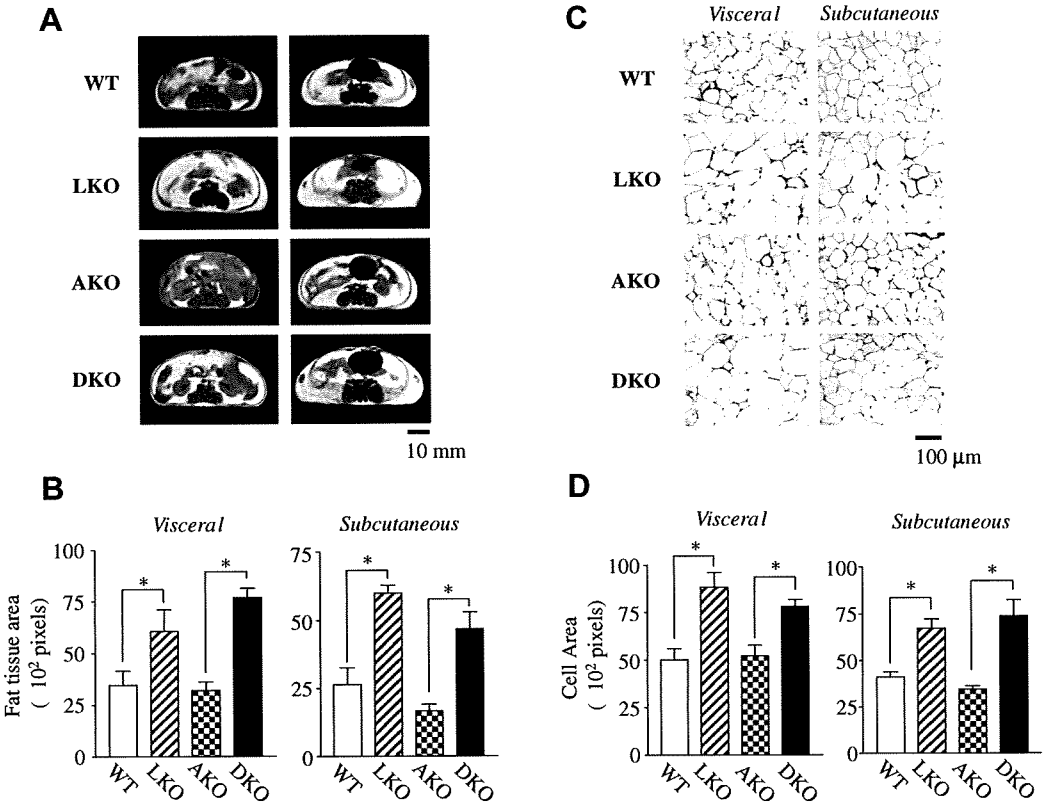

Fig. 1. (A) Abdominal open MRI transverse section of 20-week-old mice (maintained on a high-fat diet for 12 weeks). Left panel: center of the right kidney level; right panel: urinary bladder level. (B) Quantitative analyses of visceral and subcutaneous fat compartments. Areas of fat tissue were calculated as described in Methods. Data represent means ± SE ($n = 6$–8; *$P < 0.01$). (C) Representative hematoxylin–eosin-stained sections of visceral and subcutaneous fat in WT and LKO mice. Adipocyte sizes were calculated as described in Methods. Data represent means ± SE ($n = 6$; *$P < 0.01$).

were similar to the analysis of fat tissue weight obtained from sacrificed mice (data not shown).

We also compared the adipocyte sizes among mice. Adipocytes in visceral and subcutaneous fat isolated from *l-pgds*-deficient mice were significantly larger in size than those from WT and AKO mice (Fig. 1C and D).

Effect of l-pgds deficiency on atherosclerosis

Next, we evaluated the effect of *l-pgds* deficiency on atherosclerosis by investigating lipid depositions in the aortic wall and in cross-sections of the aortic root. As shown in Fig. 2A, Oil-Red-O staining in the longitudinally opened aortas showed a significant increase in atherosclerotic lesion area in LKO mice compared with WT mice after 20 weeks of high-fat diet feeding. Although greater increases in lipid deposition were observed in AKO and DKO mice, this was not statistically significant. Similarly, Oil-Red-O-stained atherosclerotic plaque area in the aortic root was increased in LKO mice compared with WT mice (Fig. 2B), but there was no difference between AKO and DKO mice (data not shown).

Effects of l-pgds deficiency on inflammatory response

The modulation of vascular remodeling mediated by inflammation is a key event in the progression of atherosclerosis. It has been reported that L-PGDS and its enzymatic products

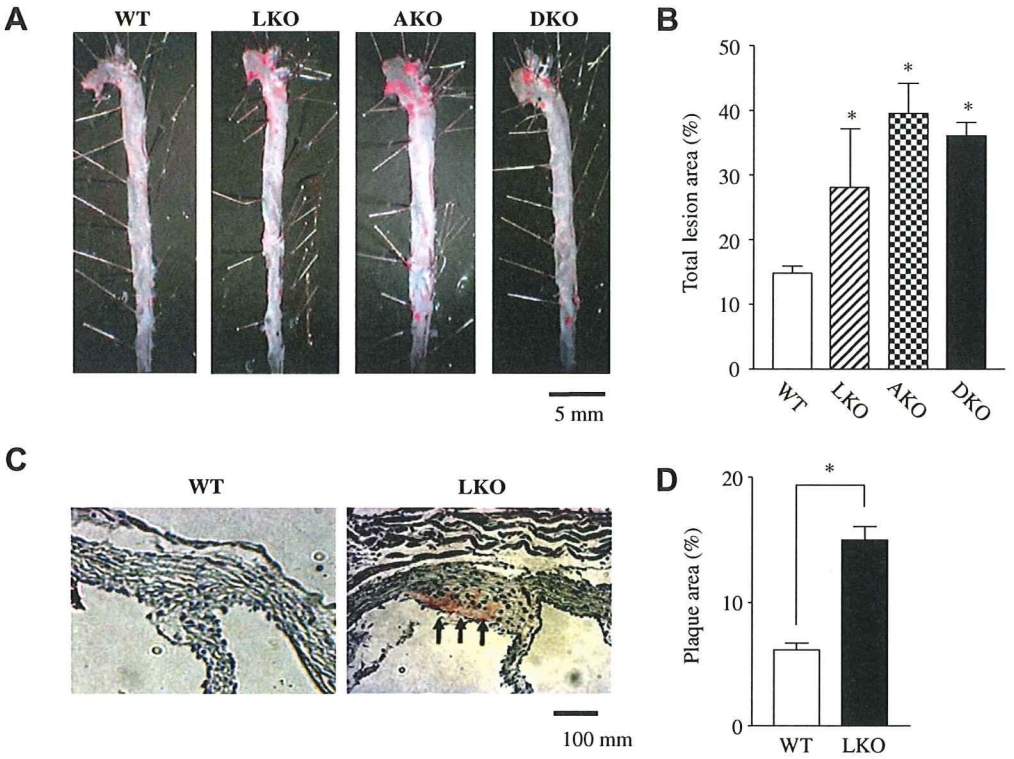

Fig. 2. Atherosclerotic lesions in 28-week-old mice (maintained on a high-fat diet for 20 weeks). (A) Lipid depositions in the aortic wall. Representative photomicrographs of longitudinally opened aortas between the subclavian and iliac branches stained with Oil-Red-O. (B) Quantitative analyses of lipid deposition in the aortic arch calculated as the percentage of the lesion area of the total vascular wall. Data represent means ± SE ($n = 6$; $^{*}P < 0.05$ vs WT). (C) Atherosclerotic lesions in the aortic root. Representative cross-sections of the aortic root stained with Oil-Red-O and hematoxylin in WT and LKO mice (arrows: lipid staining in red). (D) Quantitative analyses of atherosclerotic lesions calculated as the percentage of the Oil-Red-O stained area of the total aortic root. Data represent means ± SE for lesion area in five sections for each animal ($n = 6$; $^{*}P < 0.01$).

PGD_2/PGJ_2 have anti-inflammatory actions [7]. Therefore, to examine the effect of *l-pgds* deficiency on inflammation, we compared the infiltration of macrophages in the atherosclerotic lesions in aortic root sections between WT and LKO mice. The number of macrophages stained with anti-CD68 antibody was increased in LKO mice compared with WT mice (Fig. 3A). Furthermore, as shown in Fig. 3B, the expression of pro-inflammatory cytokines such as monocyte chemoattractant protein-1 (MCP-1) and interleukin-1β (IL-1β) in aortic root sections were also markedly enhanced in LKO mice.

Discussion

Here, we showed that *l-pgds* deficiency increases body weight, which is accompanied with an increase in fat tissue volume in a high-fat environment. *l-pgds* deficiency also facilitates atherosclerosis, although this effect occurred to a lesser than in *apo E* deficiency.

The association between L-PGDS and obesity has not been well studied. However, several previous studies suggest that downstream PGs of L-PGDS, i.e., PGD_2 and PGJ_2 contribute to adipocyte differentiation or lipid metabolism, both of which are important in the pathogenesis of obesity through activation of PPARs. In particular, 15d-PGJ_2 stimulates the differentiation of adipose cells through PPARγ, which is abundantly expressed in adipocytes and functions as a key regulator of adipocyte differentiation. Considering these observations, the lack of *l-pgds* may inhibit downstream PG generation in adipose tissue, resulting in the enlargement of adipocytes and concomitant increase in fat tissue volume. Further studies are required to clarify the role of L-PGDS in the pathogenesis of obesity.

On the other hand, PPARγ plays a major role in insulin sensitivity. PPARγ increases small adipocytes by stimulating adipocyte differentiation and enhances expression of the insulin-sensitizing hormone adiponectin. A previous study [17] reported that LKO mice fed a diabetogenic diet were insulin resistant, glucose intolerant and had low serum adiponectin levels. In our study, the high-fat diet increased body weight and induced fat cell enlargement in LKO mice; however, it did not have a significant effect on insulin sensitivity or serum adiponectin levels. Although we are not able to fully explain this discrepancy, differences in diet compositions might be responsible for the inconsistent results. Very recently, the same group reported that L-PGDS stimulates glucose transport via enhanced translocation of the insulin-responsive glucose transporter GLUT4 [18]. However, since there are no other reports to have examined the effect of L-PGDS on glucose metabolisms, further studies are required to clarify this issue.

Because L-PGDS belongs to the lipocalin superfamily, a group of proteins that bind and transport small lipophilic molecules, L-PGDS may play a role in lipid transport. Indeed, we found an association between L-PGDS and serum lipid levels in the clinical studies. Serum L-PGDS levels were inversely associated with HDL-cholesterol [13] and a gene polymorphism of human *l-pgds* gene (4111 A>C) was associated with HDL-cholesterol levels [14]. In the present study, LKO mice showed relatively lower HDL-cholesterol and higher LDL-cholesterol levels, although these findings were not statistically significant. Based on these observations, even if L-PGDS contributes to lipid metabolism, its role does not seem to be important.

Our data also provide evidence for the atheroprotective functions of L-PGDS. Although the data were preliminary, Ragolia et al. [17] reported that LKO mice fed a diabetogenic diet showed

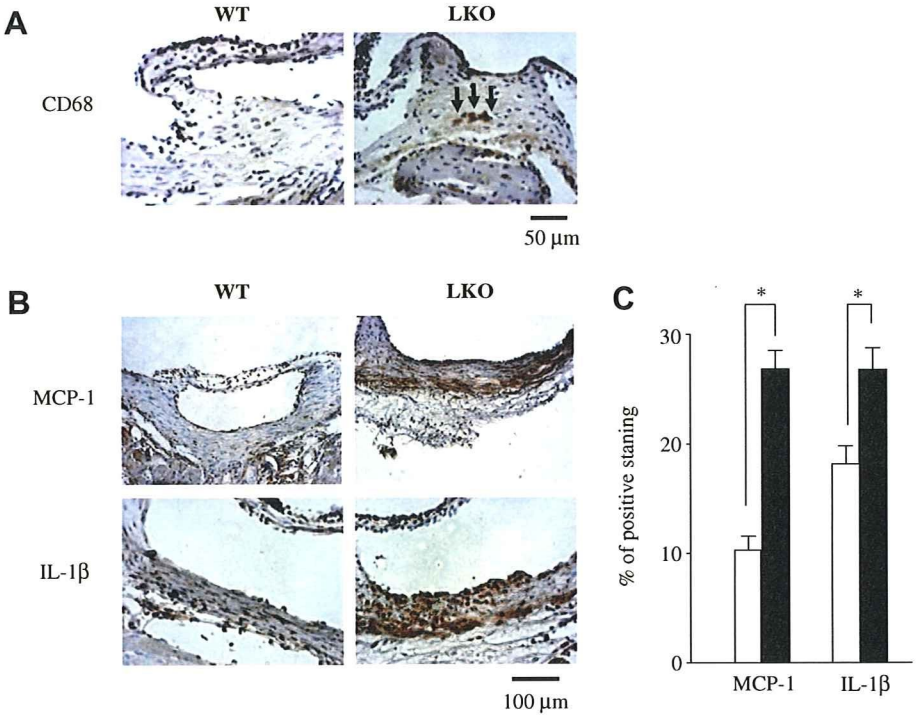

Fig. 3. (A) Immunohistochemical staining for CD68 in WT and LKO mice. Arrows indicate stained macrophages. (B) Immunohistochemical staining for MCP-1 and IL-1β in WT and LKO mice. (C) Quantitative analyses of the cell areas that stained positive for MCP-1 and IL-1β in WT mice (open bars) and LKO mice (closed bars). Data represent means ± SE for the percentage staining of the total plaque area in five sections for each animal ($n = 6$; $^{*}P < 0.01$).

progressed atherosclerosis. They attribute their results to differences in insulin resistance. Conversely, in our results, LKO mice fed a high-fat diet did not show differences in glucose homeostasis; however, they showed well-progressed atherosclerosis. Thus in our model, a mechanism other than insulin resistance seems to be associated with atherogenesis. One interesting possibility is the lack of a role of L-PGDS in inflammatory responses which play a central role in atherogenesis. The L-PGDS enzymatic product PGD_2 inhibits inducible nitric oxide synthase (NOS) [19] in vascular smooth muscle cells and suppresses the expression of pro-inflammatory mediators such as plasminogen activator inhibitor-1 [20] and vascular cell adhesion molecule-1 [21] in endothelial cells. 15d-PGJ_2 has also been shown to suppress inflammatory responses, which are dependent on or independent of PPARγ. 15d-PGJ_2 inhibits macrophage activation [22], production of monocyte inflammatory cytokines [23] and biologic functions of human natural killer cells [24]. 15d-PGJ_2 has also been shown to suppress inducible NOS expression [22]. In the present study, an increase in macrophage infiltration in the aortic root was observed in LKO mice. In support of this observation, the expression of MCP-1 which mediates monocyte recruitment to sites of inflammation and a pro-inflammatory cytokine, IL-1β, was enhanced in atherosclerotic lesions. These findings suggest that, in the vascular wall, *l-pgds* deficiency facilitates atherogenesis due to the lack of anti-inflammatory effects.

Taken together, we found that deletion of the *l-pgds* gene induces obesity in high cholesterol conditions in mice. *l-pgds* deficiency also resulted in highly progressed atherosclerosis by enhancing inflammatory responses. Our data suggest the potential anti-obese and atheroprotective effects of L-PGDS.

Acknowledgments

We are grateful to Yuko Kubota for technical assistance. This study was supported by grants from the Ministry of Education, Culture, Sports, Science and Technology (Wakate B, No. 18790178) and Uehara Foundation.

References

[1] Y. Kikawa, S. Narumiya, M. Fukushima, H. Wakatsuka, O. Hayaishi, 9-Deoxy-$\Delta^9,\Delta^{12\text{-}13,14}$-dihydroprostaglandin D_2, a metabolite of prostaglandin D_2 formed in human plasma, Proc. Natl. Acad. Sci. USA 81 (1984) 1317–1321.
[2] Y. Urade, O. Hayaishi, Prostaglandin D_2 and sleep regulation, Biochim. Biophys. Acta 1436 (1999) 606–615.
[3] O. Hayaishi, Y. Urade, Prostaglandin D_2 in sleep-wake regulation: recent progress and perspectives, Neuroscientist 8 (2002) 12–15.
[4] N. Eguchi, T. Minami, N. Shirafuji, Y. Kanaoka, T. Tanaka, A. Nagata, N. Yoshida, Y. Urade, S. Ito, O. Hayaishi, Lack of tactile pain (allodynia) in lipocalin-type prostaglandin D synthase-deficient mice, Proc. Natl. Acad. Sci. USA 96 (1999) 726–730.
[5] Y. Taba, T. Sasaguri, M. Miyagi, T. Abumiya, Y. Miwa, T. Ikeda, M. Mitsumata, Fluid shear stress induces lipocalin-type prostaglandin D_2 synthase expression in vascular endothelial cells, Circ. Res. 86 (2000) 967–973.
[6] T. Sasaguri, Y. Miwa, Prostaglandin J_2 family and the cardiovascular system, Curr. Vasc. Pharmacol. 2 (2004) 103–114 (Review).
[7] B.M. Forman, P. Tontonoz, J. Chen, R.P. Brun, B.M. Spiegelman, R.M. Evans, 15-Deoxy-$\Delta^{12,14}$-prostaglandin J_2 is a ligand for the adipocyte determination factor PPAR gamma, Cell 83 (1995) 803–812.
[8] S.A. Kliewer, J.M. Lenhard, T.M. Willson, I. Patel, D.C. Morris, J.M. Lehmann, A prostaglandin J_2 metabolite binds peroxisome proliferator-activated receptor gamma and promotes adipocyte differentiation, Cell 83 (1995) 813–819.
[9] Y. Miwa, T. Sasaguri, H. Inoue, Y. Taba, A. Ishida, T. Abumiya, 15-Deoxy-$\Delta^{12,14}$-prostaglandin J_2 induces G_1 arrest and differentiation marker expression in vascular smooth muscle cells, Mol. Pharmacol. 58 (2000) 837–844.
[10] Y. Miwa, F. Takahashi-Yanaga, S. Morimoto, T. Sasaguri, Involvement of clusterin in 15-deoxy-$\Delta^{12,14}$-prostaglandin J_2-induced vascular smooth muscle cell differentiation, Biochem. Biophys. Res. Commun. 319 (2004) 163–168.
[11] N. Hirawa, Y. Uehara, M. Yamakado, Y. Toya, T. Gomi, T. Ikeda, Y. Eguchi, M. Takagi, H. Oda, K. Seiki, Y. Urade, S. Umemura, Lipocalin-type prostaglandin d synthase in essential hypertension, Hypertension 39 (2002) 449–454.
[12] K. Hamano, Y. Totsuka, M. Ajima, T. Gomi, T. Ikeda, N. Hirawa, Y. Eguchi, M. Yamakado, M. Takagi, H. Nakajima, H. Oda, K. Seiki, N. Eguchi, Y. Urade, Y. Uehara, Blood sugar control reverses the increase in urinary excretion of prostaglandin D synthase in diabetic patients, Nephron 92 (2002) 77–85.
[13] Y. Miwa, H. Oda, Y. Shiina, K. Shikata, M. Tsushima, S. Nakano, T. Maruyama, S. Kyotani, N. Eguchi, Y. Urade, F. Takahashi-Yanaga, S. Morimoto, T. Sasaguri, Association of serum lipocalin-type prostaglandin D synthase levels with

subclinical atherosclerosis in untreated asymptomatic subjects, Hypertens. Res. 31 (2008) 1939–1947.
[14] Y. Miwa, S. Takiuchi, K. Kamide, M. Yoshii, T. Horio, C. Tanaka, M. Banno, T. Miyata, T. Sasaguri, Y. Kawano, Identification of gene polymorphism in lipocalin-type prostaglandin D synthase and its association with carotid atherosclerosis in Japanese hypertensive patients, Biochem. Biophys. Res. Commun. 322 (2004) 428–433.
[15] T. Björnheden, B. Jakubowicz, M. Levin, B. Odén, S. Edén, L. Sjöström, M. Lönn, Computerized determination of adipocyte size, Obes. Res. 12 (2004) 95–105.
[16] E.M. Rubin, R.M. Krauss, E.A. Spangler, J.G. Verstuyft, S.M. Clift, Inhibition of early atherogenesis in transgenic mice by human apolipoprotein AI, Nature 353 (1991) 265–267.
[17] L. Ragolia, T. Palaia, C.E. Hall, J.K. Maesaka, N. Eguchi, Y. Urade, Accelerated glucose intolerance, nephropathy, and atherosclerosis in prostaglandin D_2 synthase knock-out mice, J. Biol. Chem. 280 (2005) 29946–29955.
[18] L. Ragolia, C.E. Hall, T. Palaia, Lipocalin-type prostaglandin D_2 synthase stimulates glucose transport via enhanced GLUT4 translocation, Prostaglandins Other Lipid Mediat. 87 (2008) 34–41.
[19] H. Nagoshi, Y. Uehara, F. Kanai, S. Maeda, T. Ogura, A. Goto, T. Toyo-Oka, H. Esumi, T. Shimizu, M. Omata, Prostaglandin D_2 inhibits inducible nitric oxide synthase expression in rat vascular smooth muscle cells, Circ. Res. 82 (1998) 204–209.
[20] H. Negoro, W.S. Shin, R. Hakamada-Taguchi, N. Eguchi, Y. Urade, A. Goto, T. Toyo-Oka, T. Fujita, M. Omata, Y. Uehara, Endogenous prostaglandin D_2 synthesis reduces an increase in plasminogen activator inhibitor-1 following interleukin stimulation in bovine endothelial cells, J. Hypertens. 20 (2002) 1347–1354.
[21] H. Negoro, W.S. Shin, R. Hakamada-Taguchi, N. Eguchi, Y. Urade, A. Goto, T. Toyo-Oka, T. Fujita, M. Omata, Y. Uehara, Endogenous prostaglandin D_2 synthesis decreases vascular cell adhesion molecule-1 expression in human umbilical vein endothelial cells, Life Sci. 78 (2005) 22–29.
[22] M. Ricote, A.C. Li, T.M. Willson, C.J. Kelly, C.K. Glass, The peroxisome proliferator-activated receptor-gamma is a negative regulator of macrophage activation, Nature 391 (1998) 79–82.
[23] C. Jiang, A.T. Ting, B. Seed, PPAR-gamma agonists inhibit production of monocyte inflammatory cytokines, Nature 391 (1998) 82–86.
[24] X. Zhang, M.C. Rodriguez-Galan, J.J. Subleski, J.R. Ortaldo, D.L. Hodge, J.M. Wang, O. Shimozato, D.A. Reynolds, H.A. Young, Peroxisome proliferator-activated receptor-gamma and its ligands attenuate biologic functions of human natural killer cells, Blood 104 (2004) 3276–3284.

J Pharmacol Sci 109, 179 – 183 (2009)

Journal of Pharmacological Sciences

Forum Minireview

Drug Development Targeting the Glycogen Synthase Kinase-3β (GSK-3β)-Mediated Signal Transduction Pathway: Inhibitors of the Wnt/β-Catenin Signaling Pathway as Novel Anticancer Drugs

Fumi Takahashi-Yanaga[1,*] and Toshiyuki Sasaguri[1]

[1]*Department of Clinical Pharmacology, Faculty of Medical Sciences, Kyushu University, Fukuoka 812-8582, Japan*

Received October 21, 2008; Accepted November 10, 2008

Abstract. Accumulating evidence suggests that the Wnt/β-catenin signaling pathway is often involved in oncogenesis and cancer development. Accordingly, a novel anticancer drug can be developed using inhibitors of this pathway. However, at present, there is no selective inhibitor of this pathway available as a therapeutic agent. Although all the components of the Wnt/β-catenin signaling pathway can be a target for drug development, glycogen synthase kinase-3β (GSK-3β), in particular, may be a good target because GSK-3β is an essential component of the pathway, and activation of this kinase results in the inhibition of the Wnt signaling pathway. We found that the differentiation-inducing factors (DIFs), putative morphogens for *Dictyostelium discoideum*, inhibit the Wnt/β-catenin signaling pathway via the activation of GSK-3β, resulting in the cell-cycle arrest of human cancer cell lines. In this review, we summarize our recent findings on the antiproliferative effect of DIFs and show the possibility for development of a novel anticancer drug from DIFs and their derivatives.

Keywords: Wnt/β-catenin signaling, cancer, glycogen synthase kinase-3β (GSK-3β), drug development, differentiation-inducing factor

The Wnt/β-catenin signaling pathway and GSK-3β

Cell signaling cascades activated by Wnt proteins (i.e., the Wnt signaling pathways) are well conserved through evolutionary processes across a variety of species. As well as regulating cellular processes such as proliferation, differentiation, motility, and survival /apoptosis, the Wnt signaling pathways play key roles in embryonic development and maintenance of homeostasis in mature tissues. Of four known Wnt signaling pathways, [the Wnt/β-catenin (canonical) pathway, the planar cell polarity (PCP) pathway, the Wnt/Ca^{2+} pathway, the protein kinase A pathway], the Wnt/β-catenin signaling pathway is best characterized (1 – 6).

The activity of the Wnt/β-catenin signaling pathway is dependent on the amount of β-catenin in the cytoplasm. Normally, the cytoplasmic β-catenin level is kept low through continuous ubiquitin-proteasome system–mediated degradation, which is regulated by a multiprotein complex containing axin, adenomatous polyposis coli (APC), and glycogen synthase kinase-3β (GSK-3β).

GSK-3β is a cytoplasmic serine/threonine protein kinase that is known to play central roles in a variety of biological processes including a number of signaling pathways such as the Wnt/β-catenin, Hedgehog, Notch, and insulin signaling pathways (7). The activity of GSK-3β is decreased by the phosphorylation of Ser^9 and several studies have shown that Ser^9 in GSK-3β is phosphorylated by Akt, a serine/threonine kinase that is activated by phosphatidylinositol 3-kinase (PI3K), mitogen-activated protein kinase-activated protein kinase-1 (MAPKAP-K1), a protein kinase downstream of the mitogen-activated protein kinase (MAPK) cascade, and p70 ribosomal S6 kinase-1 (7 – 9).

In the Wnt/β-catenin signaling pathway, GSK-3β mediates the degradation of β-catenin molecules by phosphorylating specific amino acid residues, which marks the protein to trigger its degradation by the 26S

*Corresponding author. yanaga@clipharm.med.kyushu-u.ac.jp
Published online in J-STAGE on January 29, 2009 (in advance)
doi: 10.1254/jphs.08R28FM

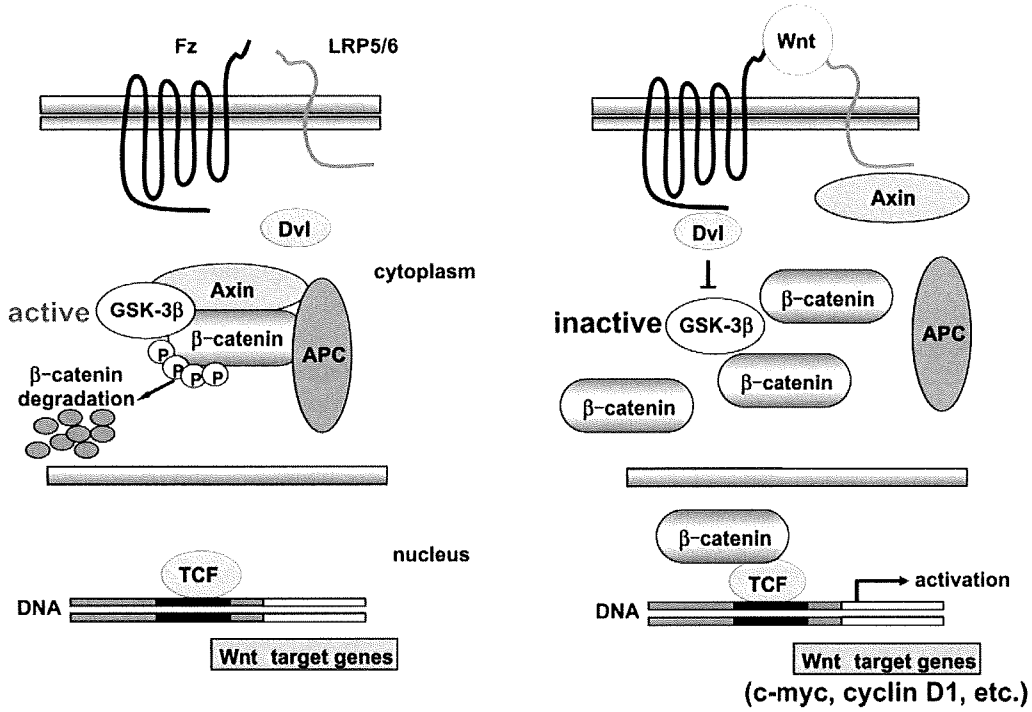

Fig. 1. The Wnt/β-catenin signaling pathway. In the absence of Wnt, β-catenin binds to the protein complex formed by axin, APC, and GSK-3β and then is phosphorylated by GSK-3β, resulting in its degradation by the 26S proteasome system (left). Wnt binds to the receptor Fz and the co-receptor LRP5/6, and these receptors mediate signal transduction in cells. GSK-3β and CK1α are inhibited by activated Dvl; thus β-catenin escapes phosphorylation. Unphosphorylated β-catenin accumulates in the cytoplasm and translocates to the nucleus. In the nucleus, β-catenin activates the transcription of target genes together with TCF (right). Fz, Frizzled; LRP, low-density lipoprotein receptor–related protein; Dvl, disheveled; APC, adenomatous polyposis coli; GSK-3β, glycogen synthase kinase-3β; TCF, T-cell factor.

proteasome complex (10, 11). After the Wnt proteins bind to the receptor complex Frizzleds/low-density lipoprotein receptor–related protein (Fz/LRP), cytoplasmic disheveled (Dvl), a protein downstream of the receptor complex, is phosphorylated and inhibits GSK-3β by causing their retention at the scaffolding protein axin, resulting in the accumulation of non-phosphorylated β-catenin in the cytoplasm. Non-phosphorylated β-catenin avoids degradation and translocates into the nucleus. In the nucleus, β-catenin forms a complex with the transcription factor TCF and induces the transcription of downstream target genes (1 – 3). Thus GSK-3β plays a critical role in the regulation of Wnt/β-catenin target gene expression by controlling the level of cytoplasmic β-catenin (Fig. 1).

Cyclin D1 and GSK-3β

Since several oncogenes are included amongst the target genes, constitutive activation of the Wnt/β-catenin signaling pathway can lead to cancer (12). One oncogene, the cyclin D1 gene CCND1, is a well-known Wnt/β-catenin target gene.

The cell cycle progresses through four sequential phases, namely, gap 1 (G1), synthesis (S), gap 2 (G2), and mitosis (M) phases. Passage through the cell cycle is strictly controlled by cyclin/cyclin-dependent kinase (CDK) complexes. During the G1 phase, cells need to decide whether to advance towards another division or withdraw from the cell cycle into the quiescence phase (G0) in response to extracellular signals. The point at which this decision is made is called the restriction point. Cyclin D (D1, D2, and D3) act as a mitogenic signal sensor and is expressed as a delayed early response to many mitogenic signals, which forces cells to enter the proliferative cycle from the G0 phase (13, 14). The cyclin D mRNA level is dramatically increased following mitogenic stimulation, and both mRNA and protein levels of cyclin D1 are strictly regulated after induction. Cyclin D forms a complex with and functions as a regulatory subunit of CDK4 or 6, the activity of which is required for the transition from the G1 phase to the S phase (Fig. 2).

In tumor cells, genes encoding the proteins that directly regulate the cell cycle are often quantitatively altered. Among these proteins, cyclin D1 is strongly

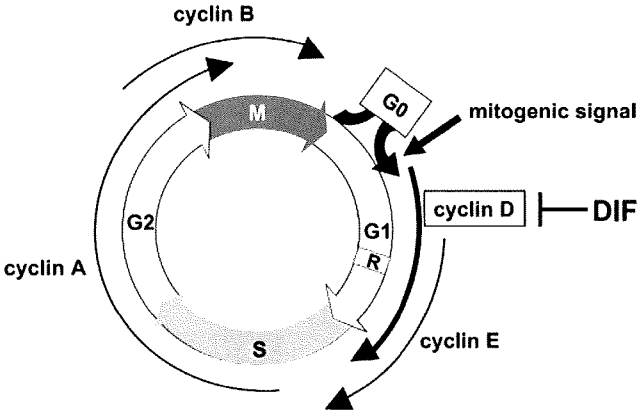

Fig. 2. Schematic representation of the mammalian cell cycle and its regulatory molecules. The cell cycle progresses through four sequential phases, gap 1 (G1), synthesis (S), gap 2 (G2), and mitosis (M) phases. Passage through the cell cycle is controlled by cyclin /cyclin-dependent kinase complexes and each cyclin exhibits a characteristic pattern of expression and degradation. Among cyclins, cyclin D acts as a mitogenic signal sensor and is expressed as an early response to many mitogenic signals, which forces cells to enter the proliferative cycle from the G0 phase. DIFs inhibit mammalian cell proliferation by suppressing the expression of cyclin D1 mRNA and protein. R, restriction point.

implicated in oncogenesis (14). Amplification of the gene encoding cyclin D1 and overexpression of cyclin D1 protein are often found in several types of human malignant neoplasms (15 – 18). Thus cyclin D1 is particularly well known for its prominent role in driving tumorigenesis. Other members of the cyclin D family, cyclins D2 and D3, are also expressed in an overlapping and redundant fashion with cyclin D1 in all proliferating cell types and are overexpressed in human cancers, but much less commonly than cyclin D1 (19).

The level of the cyclin D1 protein is regulated by an ubiquitin-dependent mechanism throughout the progression of the cell cycle. Cyclin D1 is transported from the nucleus to the cytoplasm where it is degraded by the 26S proteasome. Although GSK-3β is a cytosolic protein, it is translocated into the nucleus when activated and phosphorylates cyclin D1 on Thr^{286}, thereby stimulating cyclin D1 turnover in response to mitogenic signals (7, 20, 21). Phosphorylation of cyclin D1 on Thr^{286} by GSK-3β facilitates its association with CRM1, which is a nuclear protein that mediates the nuclear export of proteins, resulting in the exclusion of cyclin D1 from the nucleus to initiate its proteasomal degradation (22).

As described above, cyclin D1 gene expression is activated by Wnt/β-catenin signaling, in which GSK-3β plays a critical role in its regulation, and cyclin D1 protein degradation is regulated by GSK-3β. Thus activation of GSK-3β is expected to lead to a reduction in the level of cyclin D1 mRNA at the transcriptional level and the protein at the degradation level. While many diseases, including diabetes mellitus and Alzheimer's disease, can be ameliorated by the use of GSK-3β inhibitors, cancers, especially cancers in which cyclin D1 is overexpressed, are likely to be more susceptible to pharmacological activation of GSK-3β.

Differentiation-inducing factors: modulators of the Wnt/β-catenin signaling pathway and potent anti-tumor agents

Differentiation-inducing factors (DIFs) were identified in *Dictyostelium discoideum* as the morphogens required for stalk cell differentiation (23). In the DIF family, DIF-1 [1-(3,5-dichloro-2,6-dihydroxy-4-methoxyphenyl)-1-hexanone] was the first to be identified and DIF-3, the monochlorinated analog of DIF-1, is a natural metabolite of DIF-1 in *Dictyostelium* (24). However, the actions of DIFs are not limited to *Dictyostelium*. They also have strong effects on mammalian cells. DIF-1 and/or DIF-3 strongly inhibit proliferation and induce differentiation in several leukemia cells, including the murine erythroleukemia cell line B8, human leukemia cell line K562, and human myeloid leukemia cell line HL-60 (25, 26). DIF-3 has been reported to have the most potent antiproliferative effect on mammalian leukemia cells among the DIF analog examined to date (27).

However, the target molecule (receptor) of DIFs is unknown and it is not clear even in *Dictyostelium* how DIFs induce antiproliferative effects and cell differentiation. DIFs are small hydrophobic molecules and are therefore expected to be able to cross cell membranes without requiring channels or carriers. In search of chemical substances applicable for the treatment of cancer and other proliferative disorders, we studied the signal transduction of DIFs in mammalian cells mainly using HeLa cells. Although the precise mechanisms underlying their antiproliferative effects are not yet known, we found that DIFs (DIF-1 and DIF-3) inhibited mammalian cell proliferation by suppressing the expression of cyclin D1 mRNA and protein through the activation of GSK-3β (28 – 31).

DIFs dephosphorylated Ser^9 of GSK-3β by an unknown mechanism and thus activated this kinase. Activated GSK-3β by DIFs induced β-catenin degradation and suppressed β-catenin/TCF–dependent transcription activity, indicating that DIFs inhibit the Wnt/β-catenin signaling pathway. We also found that DIFs reduced the activity of a reporter gene driven by the human cyclin D1 promoter (+134/–961 bp) via a TCF binding site (–75/–81 bp) (29). This result suggests that DIFs inhibited cyclin D1 mRNA expression via the inhibition of β-catenin/TCF–dependent transcription

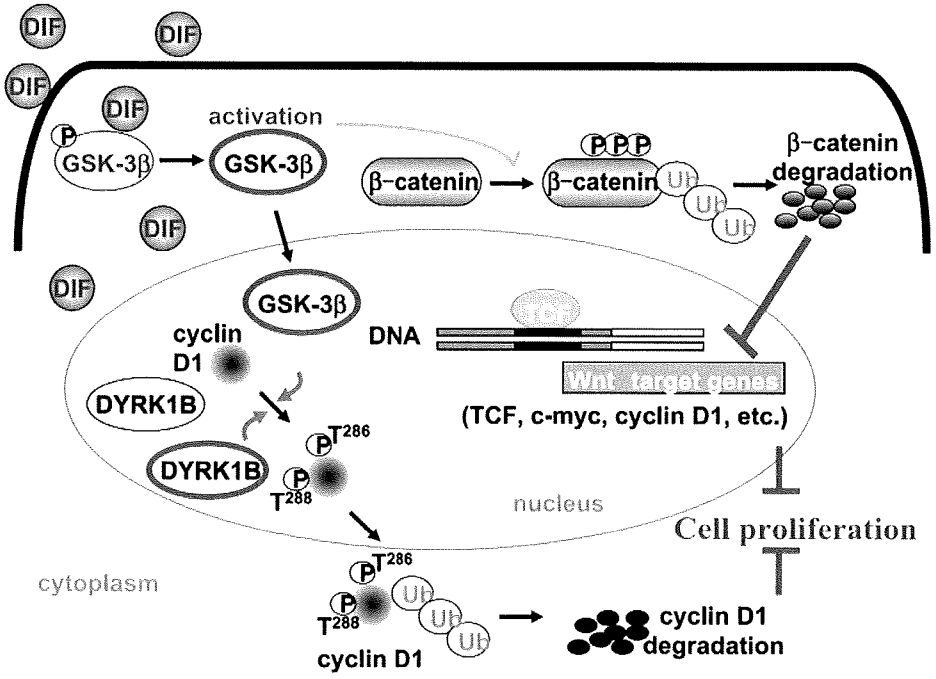

Fig. 3. DIFs action and the Wnt/β-catenin signaling pathway. DIFs enter into the cell and dephosphorylate GSK-3β at Ser^{9} by unknown mechanisms, resulting in the activation of this kinase. Activated-GSK-3β translocates into nucleus and phosphorylates Thr^{286} of cyclin D1. DIFs also activated DYRK1B, which is present in nucleus, by an unknown mechanism, and activated DYRK1B phosphorylates Thr^{288} of cyclin D1. Phosphorylated cyclin D1 is exported from the nucleus, resulting in its degradation by the 26S proteasome system after ubiquitination. Activated-GSK-3β also phosphorylates β-catenin in the cytoplasm. Phosphorylated β-catenin is degraded, resulting in the inhibition of transcription of the target genes, such as cyclin D1 and c-myc. GSK-3β, glycogen synthase kinase-3β; DYRK1B, dual-specificity tyrosine phosphorylation-regulated kinase 1B; Ub, ubiquitin.

activity. On the other hand, we also found that the activated GSK-3β translocated to the nucleus and phosphorylated cyclin D1 on Thr^{286} to trigger the degradation of cyclin D1 by an ubiquitin-dependent mechanism (28, 30, 31). Correlated with the above observations, DIFs induced G0/G1 cell cycle arrest, which was rescued by the overexpression of cyclin D1 (28), suggesting that DIFs were likely to induce cell cycle arrest by reducing the expression of cyclin D1.

Cyclin D1 degradation is facilitated by the phosphorylation of specific threonine residues, not only 286 but also 288, according to previous reports (20, 21, 32). Zou et al. (32) reported that dual-specificity tyrosine-phosphorylation–regulated kinase 1B (DYRK1B), a member of the DYRK family, phosphorylates cyclin D1 on Thr^{288}, also resulting in cyclin D1 degradation. Therefore, the effect of DIF-3 on DYRK1B was examined and it was found that not only GSK-3β but also DYRK1B was involved in the phosphorylation of cyclin D1 to trigger its degradation (31). This may have an important implication in DIFs-induced cyclin D1 degradation because DIFs induce rapid and strong degradation of cyclin D1 (within 1 h). Clarified DIFs action is summarized in Fig. 3.

The antiproliferative effect of DIFs via strong reduction of the expression level of cyclin D1 is not limited to HeLa cells, but is also common to human squamous cell carcinoma cell lines (SAS and NA) (30), human colorectal carcinoma cell line (HCT-116), and human osteosarcoma cell line (SaOS-2) (author's unpublished observation). As described above, DIFs inhibit the Wnt/β-catenin signaling pathway via the activation of GSK-3β, whereas the target molecule is not clarified. Recently, Shimizu et al. reported that calmodulin-dependent cyclic nucleotide phosphodiesterase (PDE1) could be a pharmacological target molecule for DIF-1 (33). Although this protein might not be the molecule responsible for regulation of the antiproliferative effect of DIF-1 (4), some inhibitors for PDE1 are expected to be applicable to cancer (34, 35). Taken together, it seems likely that DIFs are potent antitumor agents, and identification of the target molecule(s) for DIFs may offer ideas for the design of new anticancer drugs.

Conclusions

Cyclin D1 is a positive regulator of the cell cycle and promotes transition from the G1phase to the S phase in cooperation with CDK4 or 6. Amplification of the gene encoding cyclin D1 and overexpression of the cyclin D1 protein are frequently found in several types of human malignant neoplasms. GSK-3β plays a critical role in the regulation of the amount of cyclin D1, as this kinase is involved in both cyclin D1 mRNA transcription and ubiquitin-dependent proteolysis. We found that DIFs act as an inhibitor of the Wnt/β-catenin signaling pathway via the activation of GSK-3β, whereas the target molecule is not clarified. Therefore, DIFs could be potent antitumor agents and identification of the target molecule(s) for DIFs may offer ideas for the design of new anticancer drugs.

Acknowledgments

We would like to thank Prof. Yutaka Watanabe for providing DIFs. This work was supported by a Grant-in-Aid for Scientific Research from the Ministry of Education, Culture, Sports, Science, and Technology.

References

1 Nelson WJ, Nusse R. Convergence of Wnt, β-catenin, and cadherin pathways. Science. 2004;303:1483–1487.
2 Moon RT, Bowerman B, Boutros M, Perrimon N. The promise and perils of Wnt signaling through β-catenin. Science. 2002; 296:1644–1646.
3 Akiyama T. Wnt/β-catenin signaling. Cytokine Growth Factor Rev. 2000;11:273–282.
4 Mlodzik M. Planar cell polarization: do the same mechanisms regulate Drosophila tissue polarity and vertebrate gastrulation? Trends Genet. 2002;18:564–571.
5 Kühl M, Sheldahl LC, Park M, Miller JR, Moon RT. The Wnt/Ca^{2+} pathway: a new vertebrate Wnt signaling pathway takes shape. Trends Genet. 2000;16:279–283.
6 Chen AE, Ginty DD, Fan CM. Protein kinase A signalling via CREB controls myogenesis induced by Wnt proteins. Nature. 2005;433:317–322.
7 Cohen P, Frame S. The renaissance of GSK3. Nat Rev Mol Cell Biol. 2001;2:769–776.
8 Frame S, Cohen P. GSK3 takes centre stage more than 20 years after its discovery. Biochem J. 2001;359:1–16.
9 Cross D, Alessi DR, Cohen P, Andjelkovich M, Hemmings BA. Inhibition of glycogen synthase kinase-3 by insulin mediated by protein kinase B. Nature. 1995;378:785–789.
10 Kitagawa M, Hatakeyama S, Shirane M, Matsumoto M, Ishida N, Hattori K, et al. An F-box protein, FWD1, mediates ubiquitin-dependent proteolysis of β-catenin. EMBO J. 1999;18: 2401–2410.
11 Liu C, Li Y, Semenov M, Han C, Baeg GH, Tan Y, et al. Control of β-catenin phosphorylation/degradation by a dual-kinase mechanism. Cell. 2002;108:837–847.
12 Willert K, Jones KA. Wnt signaling: is the party in the nucleus? Genes Dev. 2006;20:1394–1404.
13 Sherr CJ. D-type cyclins. Trends Biochem Sci. 1995;20:187–190.
14 Sherr CJ. Cancer cell cycles. Science. 1996;274:1672–1677.
15 Barnes DM, Gillett CE. Cyclin D1 in breast cancer. Brest Cancer Res Treat. 1998;52:1–15.
16 Barbieri F, Lorenzi P, Ragni N, Schettini G, Bruzzo C, Pedullá F, et al. Overexpression of cyclin D1 is associated with poor survival in epithelial ovarian cancer. Oncology. 2004;66:310–315.
17 Utsunomiya T, Doki Y, Takemoto H, Shiozaki H, Yano M, Sekimoto M, et al. Correlation of β-catenin and cyclin D1 expression in colon cancers. Oncology. 2001;61:226–233.
18 Fu M, Wang C, Li Z, Sakamaki T, Pestell RG. Cyclin D1: normal and abnormal functions. Endocrinology. 2004;145:5439–5447.
19 Malumbres M, Barbacid M. To cycle or not to cycle: a critical decision in cancer. Nat Rev Cancer. 2001;1:222–231.
20 Diehl JA, Zindy F, Sherr CJ. Inhibition of cyclin D1 phosphorylation on threonine-286 prevents its rapid degradation via the ubiquitin-proteasome pathway. Genes Dev. 1997;11:957–972.
21 Diehl JA, Cheng M, Roussel MF, Sherr CJ. Glycogen synthase kinase-3β regulates cyclin D1 proteolysis and subcellular localization. Genes Dev. 1998;12:3499–3511.
22 Alt JR, Cleveland JL, Hannink M, Diehl JA. Phosphorylation-dependent regulation of cyclin D1 nuclear export and cyclin D1-dependent cellular transformation. Genes Dev. 2000;15:3102–3114.
23 Morris HR, Taylor GW, Masento MS, Jermyn KA, Kay RR. Chemical structure of the morphogen differentiation inducing factor from Dictyostelium discoideum. Nature. 1987;328:811–814.
24 Morris HR, Masento MS, Taylor GW, Jermyn KA, Kay RR. Structure elucidation of two differentiation inducing factors (DIF-2 and DIF-3) from the cellular slime mould Dictyostelium discoideum. Biochem J. 1988;249:903–906.
25 Asahi K, Sakurai A, Takahashi N, Kubohara Y, Okamoto K, Tanaka Y. DIF-1, morphogen of Dictyostelium discoideum, induces the erythroid differentiation in murine and human leukemia cells. Biochem Biophys Res Commun. 1995;208: 1036–1039.
26 Kubohara Y. DIF-1, putative morphogen of D. discoideum, suppresses cell growth and promotes retinoic acid-induced cell differentiation in HL-60. Biochem Biophys Res Commun. 1997;236:418–422.
27 Kubohara Y. Effects of differentiation-inducing factors of Dictyostelium discoideum on human leukemia K562 cells: DIF-3 is the most potent anti-leukemic agent. Eur J Pharmacol. 1999;381:57–62.
28 Takahashi-Yanaga F, Taba Y, Miwa Y, Kubohara Y, Watanabe Y, Hirata M, et al. Dictyostelium differentiation-inducing factor-3 activates glycogen synthase kinase-3β and degrades cyclin D1 in mammalian cells. J Biol Chem. 2003;278:9663–9670.
29 Yasmin T, Takahashi-Yanaga F, Mori J, Miwa Y, Hirata M, Watanabe Y, et al. Differentiation-inducing factor-1 suppresses gene expression of cyclin D1 in tumor cells. Biochem Biophys Res Commun. 2005;338:903–909.
30 Mori J, Takahashi-Yanaga F, Miwa Y, Watanabe Y, Hirata M, Morimoto S, et al. Differentiation-inducing factor-1 induces cyclin D1 degradation through the phosphorylation of Thr^{286} in squamous cell carcinoma. Exp Cell Res. 2005;310:426–433.
31 Takahashi-Yanaga F, Mori J, Matsuzaki E, Watanabe Y, Hirata M, Miwa Y, et al. Involvement of GSK-3β and DYRK1B in differentiation-inducing factor-3-induced phosphorylation of cyclin D1 in HeLa cells. J Biol Chem. 2006;281:38489–38497.
32 Zou Y, Ewton DZ, Deng X, Mercer SE, Friedman E. Mirk/dyrk1B kinase destabilizes cyclin D1 by phosphorylation at threonine 288. J Biol Chem. 2004;279:27790–27798.
33 Shimizu K, Murata T, Tagawa T, Takahashi K, Ishikawa R, Abe Y, et al. Calmodulin-dependent cyclic nucleotide phosphodiesterase (PDE1) is a pharmacological target of differentiation-inducing factor-1, an antitumor agent isolated from Dictyostelium. Cancer Res. 2004;64:2568–2571.
34 Kakkar R, Raju RV, Sharma RK. Calmodulin-dependent cyclic nucleotide phosphodiesterase (PDE1). Cell Mol Life Sci. 1999; 55:1164–1186.
35 Lerner A, Kim DH, Lee R. The cAMP signaling pathway as a therapeutic target in lymphoid malignancies. Leuk Lymphoma. 2000;37:39–51.

J Pharmacol Sci 109, 456 – 458 (2009)

Journal of Pharmacological Sciences

Short Communication

Propyl Gallate, a Strong Antioxidant, Increases the Ca^{2+} Sensitivity of Cardiac Myofilament

Naoto Tadano[1,2], Sachio Morimoto[1,*], Fumi Takahashi-Yanaga[1], Yoshikazu Miwa[1], Iwao Ohtsuki[3], and Toshiyuki Sasaguri[1]

[1]*Department of Clinical Pharmacology, Graduate School of Medical Sciences, Kyushu University, Fukuoka 812-8582, Japan*
[2]*Central Reserch Laboratory, Zenyaku Kogyo Co., Ltd., Tokyo 178-0062, Japan*
[3]*Department of Physiology, The Jikei University School of Medicine, Tokyo 105-8461, Japan*

Received September 25, 2008; Accepted December 1, 2008

Abstract. Ca^{2+} sensitizers are cardiotonic agents that directly increase the Ca^{2+} sensitivity of cardiac myofilament. To find a novel Ca^{2+} sensitizer, we have screened a group of phenolic compounds by examining their effects on the Ca^{2+}-dependent force generation in cardiac muscle fibers. We found that propyl gallate, a strong antioxidant, increased the Ca^{2+} sensitivity of cardiac myofilament in a dose-dependent and reversible manner. The present study indicates that propyl gallate is a novel type of Ca^{2+} sensitizer with antioxidant activity, which might be more beneficial for the treatment of congestive heart failure associated with oxidative stress than existing Ca^{2+} sensitizers.

Keywords: propyl gallate, Ca^{2+} sensitizer, antioxidant

Ca^{2+} sensitizers are cardiotonic agents that elicit a positive inotropic effect via an increase in the sensitivity of cardiac myofilaments to Ca^{2+} (1, 2). These agents have advantages of avoiding Ca^{2+} overloading and oxidative stress, which could be caused by other cardiotonic agents such as β-receptor agonists through increased myocardial oxygen consumption, in the treatment of congestive heart failure (CHF) (3, 4). Ca^{2+} sensitizers have also been shown to be beneficial for the treatment of dilated cardiomyopathy associated with a decrease in the myofilament Ca^{2+} sensitivity (5). Oxidative stress is involved in myocardial ischemia/reperfusion injury, and antioxidants have been shown to attenuate cardiac dysfunction during post ischemic myocardial stunning (6) and oxidative stress–induced myocardial injury (7) by preventing the accumulation of oxygen free radicals. In this study, we screened a group of phenolic compounds to find a novel type of Ca^{2+} sensitizer.

Membrane permeabilized (skinned) cardiac muscle fibers were prepared from the left ventricular trabeculae of young male albino rabbits (2 – 2.5 kg), and force measurements were performed as described previously (8). Briefly, small bundles (0.5 – 1-mm-wide and 5 – 7-mm-long) of trabeculae tied to glass capillary tubes were skinned with relaxing solution containing 50% glycerol. A small fiber (about 200 μm in diameter) dissected from the stock-skinned trabeculae was mounted in a thermostatically controlled chamber with a capacity of 0.2 ml. The fiber length between hooks was about 1 mm, and the resting sarcomere length was set to 2.3 μm by using laser diffraction. The force generated by skinned muscle fibers was measured at 25°C with a strain gauge (UL-2GR; Minebea, Nagano). The relaxing solution consisted of 50 mM MOPS/KOH (pH 7.0), 100 mM KCl, 6 mM MgCl2, 5 mM ATP, 4 mM EGTA, 0.5 mM DTT, 10 mM creatinine phosphate, and 35 units/ml creatine kinase.

Trolox (water-soluble derivative of tocopherol) was purchased from Sigma (St. Louis, MO, USA). Curcumin, quercetin, chrologenate, gallate monohydrate, dodecyl gallate, and propyl gallate were purchased from Wako Pure Chemical Industries (Osaka). All phenolic compounds were dissolved in dimethylsulfoxide (DMSO) and used at the final concentration of 0.1% DMSO.

Antioxidant activities of phenolic compounds were

*Corresponding author. morimoto@med.Kyushu-u.ac.jp
Published online in J-STAGE
doi: 10.1254/jphs.08266SC

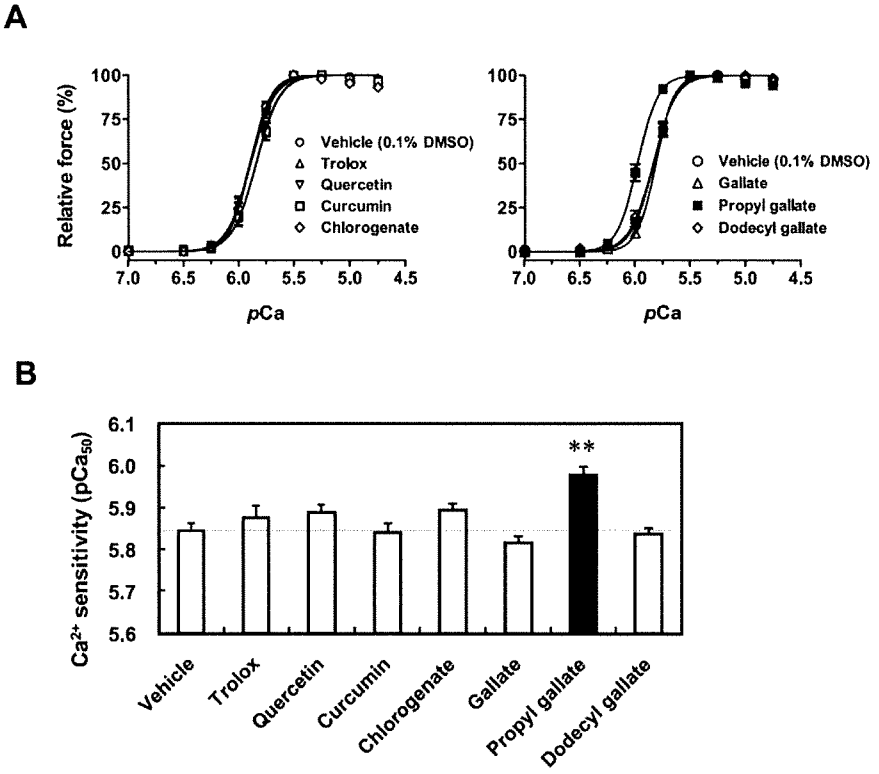

Fig. 1. Effects of phenolic compounds on the force generation in skinned cardiac muscle fibers. A: Force–pCa relationships determined in the presence of 100 μM phenolic compounds. B: Effects of phenolic compounds (100 μM) on the Ca^{2+} sensitivity (pCa$_{50}$) of force generation. The force–pCa relationship was determined only once for a given muscle fiber by cumulatively increasing [Ca^{2+}] from pCa7 to pCa4.75 in the presence of phenolic compound or vehicle only without pretreatment. Forces were normalized to the maximum force developed by each fiber. Data represent the means ± S.E.M. for 5 – 8 muscle fibers. **P<0.01 vs. vehicle (Student's t-test).

evaluated by their effects of scavenging stable free radical, 1,1-diphenyl-2-picryl hydrazyl (DPPH), according to the method described by Shirwaikar et al. (9). Briefly, the reaction mixtures containing 10 μM DPPH and various concentrations of phenolic compounds were incubated for 10 min at room temperature in the dark, and then the antioxidant activity was calculated as a percent reduction of the light absorbance of DPPH at 517 nm.

Effects of phenolic antioxidant compounds, trolox, curcumin, quercetin, chrologenate, gallate, dodecyl gallate, and propyl gallate, were examined at 100 μM on the Ca^{2+}-dependent force generation in skinned cardiac muscle fibers (Fig. 1). Propyl gallate was found to shift the force–pCa relationship leftward with a significant increase in the half-maximally activating pCa (pCa$_{50}$, an index of Ca^{2+} sensitivity), while the other compounds had no significant effects on the force–pCa relationship.

Propyl gallate increased the Ca^{2+} sensitivity of force generation in skinned cardiac muscle fibers in a dose-dependent manner (Fig. 2: A and B), with statistically significant increase in Ca^{2+} sensitivity being detected above 100 μM (Fig. 2C). The Ca^{2+}-sensitizing effect of propyl gallate was reversible and lost immediately after washout (data not shown), and its potency appears to be lower than that of the commercially launched Ca^{2+}-sensitizer pimobendan (cf. supplementary data in ref. 5). All the phenolic antioxidant compounds examined had no significant effects on the maximum force and the slope of force–pCa relationship (i.e., Hill coefficient) in skinned cardiac muscle fibers (data not shown). Propyl gallate had a strong antioxidant activity, which was similar to those of other phenolic compounds, trolox, curcumin, and gallate, when evaluated by their free radical (DPPH) scavenging effects (Fig. 3).

Free radical injury is involved in the pathology of congestive heart failure (CHF); CHF patients have an increased level of plasma lipid peroxide, a marker of oxidative stress, and a decreased activity of glutathione peroxidase, an antioxidant enzyme. Antioxidant supplementation has been shown to improve the myocardial function and survival of CHF patients (10). Clinical therapeutic trials have shown that carvedilol, a nonselective β-adrenergic receptor antagonist with antioxidant activity, reduces the mortality among patients with severe heart failure (11), whereas bucindolol, a nonselective β-adrenergic receptor antagonist with no antioxidant activity, has no favorable effects (12). Propyl gallate is a phenolic antioxidant compound, and its chronic oral administration has been reported to offer significant protection against myocardial oxidative stress–induced injury (7). The present study revealed that this compound also has a Ca^{2+}-sensitizing effect on the cardiac

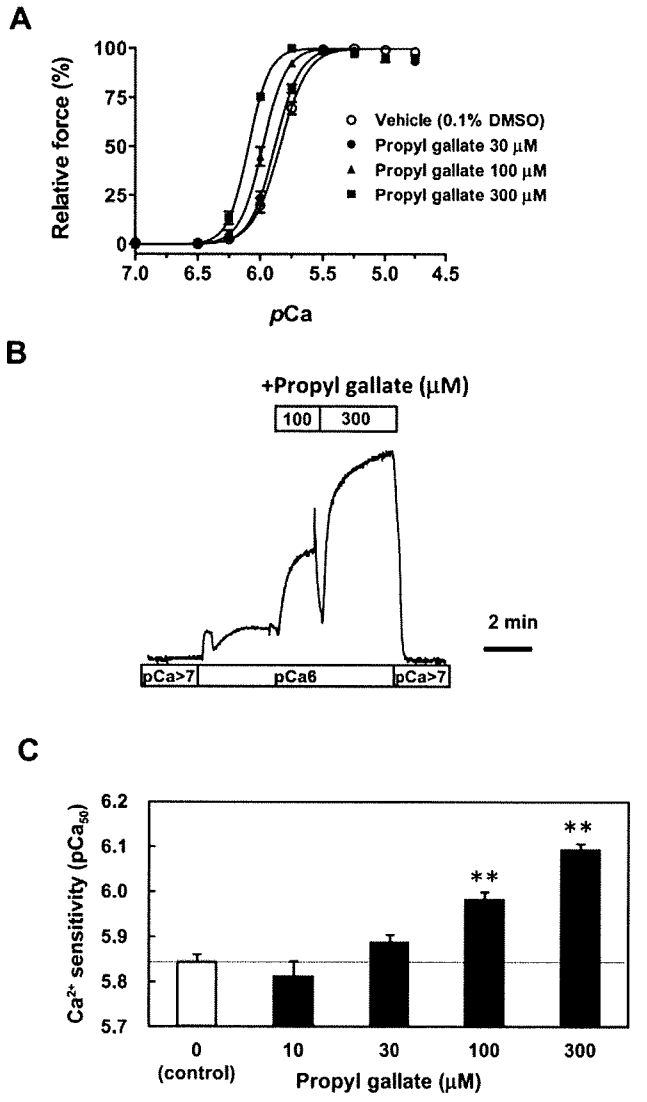

Fig. 2. Effects of propyl gallate on the force generation in skinned cardiac muscle fibers. A: Force–pCa relationships determined in the presence of 0, 10, 30, and 100 μM propyl gallate. B: Force recording showing dose-dependent Ca^{2+}-sensitizing effects of propyl gallate. C: Dose-dependent effects of propyl gallate on the Ca^{2+} sensitivity (pCa$_{50}$) of force generation. The force–pCa relationship was determined only once for a given muscle fiber by cumulatively increasing [Ca^{2+}] from pCa7 to pCa4.75 in the presence of propyl gallate or vehicle only without pretreatment. Forces were normalized to the maximum force developed by each fiber. Data represent the means ± S.E.M. for 5 – 8 muscle fibers. Statistical significance was determined by ANOVA followed by the post hoc Dunnett's multiple comparison test. $^{**}P<0.01$ vs. control.

myofilament, through which an inotropic effect would be exerted on the heart. Propyl gallate, a Ca^{2+} sensitizer with strong antioxidant activity, thus might be more beneficial for the treatment of CHF than existing Ca^{2+} sensitizers with no antioxidant activities. Further studies would be required to test this possibility.

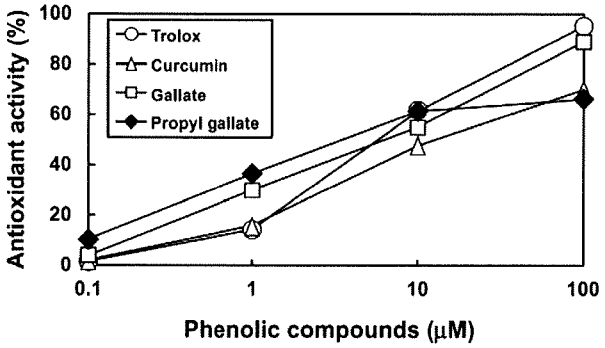

Fig. 3. Antioxidant activities of phenolic compounds. EC_{50} values of free radical (DPPH)-scavenging effects of trolox, curcumin, gallate, and propyl gallate were 8.4, 10.4, 9.0, and 1.3 μM, respectively. Data represent the means ± S.E.M. of 3 determinations.

References

1 Kass DA, Solaro RJ. Mechanisms and use of calcium-sensitizing agents in the failing heart. Circulation. 2006;113:305–315.
2 Tadano N, Morimoto S, Yoshimura A, Miura M, Yoshioka K, Sakato M, et al. SCH00013, a novel Ca^{2+} sensitizer with positive inotropic and no chronotropic action in heart failure. J Pharmacol Sci. 2005;97:53–60.
3 Shinke T, Shite J, Takaoka H, Hata K, Inoue N, Yoshikawa R, et al. Vitamin C restores the contractile response to dobutamine and improves myocardial efficiency in patients with heart failure after anterior myocardial infarction. Am Heart J. 2007;154:645.e641–e648.
4 Givertz MM, Sawyer DB, Colucci WS. Antioxidants and myocardial contractility: illuminating the "Dark Side" of β-adrenergic receptor activation? Circulation. 2001;103:782–783.
5 Du CK, Morimoto S, Nishii K, Minakami R, Ohta M, Tadano N, et al. Knock-in mouse model of dilated cardiomyopathy caused by troponin mutation. Circ Res. 2007;101:185–194.
6 Kaplan P, Matejovicova M, Herijgers P, Flameng W. Effect of free radical scavengers on myocardial function and Na^+, K^+-ATPase activity in stunned rabbit myocardium. Scand Cardiovasc J. 2005;39:213–219.
7 Karthikeyan K, Sarala Bai BR, Gauthaman K, Niranjali Devaraj S. Protective effect of propyl gallate against myocardial oxidative stress-induced injury in rat. J Pharm Pharmacol. 2005;57: 67–73.
8 Morimoto S, Yanaga F, Minakami R, Ohtsuki I. Ca^{2+}-sensitizing effects of the mutations at Ile-79 and Arg-92 of troponin T in hypertrophic cardiomyopathy. Am J Physiol. 1998;275:C200–C207.
9 Shirwaikar A, Rajendran K, Punitha IS. In vitro antioxidant studies on the benzyl tetra isoquinoline alkaloid berberine. Biol Pharm Bull. 2006;29:1906–1910.
10 Keith M, Geranmayegan A, Sole MJ, Kurian R, Robinson A, Omran AS, et al. Increased oxidative stress in patients with congestive heart failure. J Am Coll Cardiol. 1998;31:1352–1356.
11 Packer M, Coats AJ, Fowler MB, Katus HA, Krum H, Mohacsi P, et al. Effect of carvedilol on survival in severe chronic heart failure. N Engl J Med. 2001;344:1651–1658.
12 Anderson JL, Krause-Steinrauf H, Goldman S, Clemson BS, Domanski MJ, Hager WD, et al. Failure of benefit and early hazard of bucindolol for Class IV heart failure. J Card Fail. 2003;9:266–277.

Hypertension Research (2009), 1–10

www.nature.com/hr

ORIGINAL ARTICLE

The involvement of aldosterone in cyclic stretch-mediated activation of NADPH oxidase in vascular smooth muscle cells

Takahiro Ohmine[1,2], Yoshikazu Miwa[1], Fumi Takahashi-Yanaga[1], Sachio Morimoto[1], Yoshihiko Maehara[2] and Toshiyuki Sasaguri[1]

Increasing evidence suggests that aldosterone is implicated in the pathogenesis of cardiovascular diseases. We examined whether aldosterone contributes to the cyclic stretch (CS)-induced reactive oxygen species (ROS) generation in rat aortic smooth muscle cells (RASMCs). RASMCs were exposed to uniaxial CS and thereafter collected to evaluate the expressions of mRNA or protein relating aldosterone synthesis and the nicotinamide adenine dinucleotide phosphate (NADPH) oxidase activity. CS strength-dependently enhanced NADPH oxidase activity. CS induced cytochrome *P*450 aldosterone synthase (CYP11B2) and increased aldosterone synthesis but did not influence the levels of 11β-hydroxysteroid dehydrogenase 2 and mineralocorticoid receptor (MR). This CYP11B2 induction was almost completely suppressed by treatment with an extracellular signal-regulated kinase (ERK) inhibitor, U0126, whereas olmesartan, an angiotensin II (Ang II) receptor blocker (ARB), only partially suppressed CS-induced CYP11B2 expression and ERK phosphorylation. A selective MR antagonist, eplerenone (10 μmol l^{-1}), significantly attenuated the CS-induced NADPH oxidase activation even in the presence of ARBs. In conclusion, aldosterone synthesis, which is partially independent of Ang II, may have an important role in CS-stimulated ROS generation in cultured RASMCs. We also suggest the potential benefit of eplerenone in the treatment of cardiovascular diseases.
Hypertension Research advance online publication, 29 May 2009; doi:10.1038/hr.2009.76

Keywords: aldosterone; cyclic stretch; CYP11B2; eplerenone; NADPH oxidase

INTRODUCTION

Vascular smooth muscle cells (VSMCs) are persistently exposed to pulsatile stretch. Although physiological levels of pulsatile stretch may be required to maintain homeostasis in blood vessels, accumulating evidence has revealed that excessive stretch stimuli associated with hypertension promote atherosclerosis. It has been reported that mechanical stretch stimulates VSMC proliferation[1] and apoptosis,[2] and enhances the expression and activity of matrix metalloproteinase 2, which has a central role in the reorganization of the extracellular matrix.[3]

Reactive oxygen species (ROS) seem to be important mediators in atherogenesis. Increased production of ROS stimulates the oxidation of low-density lipoprotein,[4] which has a central role in the initiation and development of atherosclerosis. ROS have also been reported to promote atherosclerosis by inducing inflammation, endothelial dysfunction and abnormal VSMC proliferation.[5] Recent studies have suggested that pulsatile stretch stimulates the generation of ROS through the activation of nicotinamide adenine dinucleotide phosphate (NADPH) oxidase in human VSMCs.[3,6] Furthermore, it has been revealed that this NADPH oxidase activity is induced mainly through angiotensin II (Ang II),[7] which evokes local vascular wall inflammation by inducing the production of pro-inflammatory cytokines and chemokines, growth factors and adhesion molecules.

Aldosterone is downstream of Ang II in the renin–angiotensin–aldosterone system. Aldosterone has been considered to be synthesized mainly in the adrenal gland and implicated in blood pressure control by regulating renal sodium transport. However, recent studies have suggested that aldosterone is also synthesized in the cardiovascular system and is involved in local tissue injury such as Ang II. Indeed, patients with primary aldosteronism had a higher risk of cardiovascular events than those with essential hypertension.[8] A pharmacological blockade of aldosterone reduced cardiovascular mortality in patients with congestive heart failure.[9]

Aldosterone is synthesized from corticosterone by cytochrome *P*450 aldosterone synthase (CYP11B2) and exerts its effect by binding to mineralocorticoid receptor (MR). Although MR has almost the same affinity for glucocorticoids as cortisol and corticosterone, 11β-hydroxysteroid dehydrogenase 2 (11β-HSD2) regulates the selectivity in relation to aldosterone by transforming glucocorticoids into inactivated forms. Recent studies have indicated that CYP11B2 is expressed

[1]Faculty of Medical Sciences, Department of Clinical Pharmacology, Kyushu University, Fukuoka, Japan and [2]Faculty of Medical Sciences, Department of Surgery and Science, Kyushu University, Fukuoka, Japan
Correspondence: Dr Y Miwa, Faculty of Medical Sciences, Department of Clinical Pharmacology, Kyushu University, Fukuoka, 812-8582, Japan.
E-mail: ymiwa@clipharm.med.kyushu-u.ac.jp
Received 7 September 2008; revised 23 April 2009; accepted 30 April 2009

in VSMCs[10] and that aldosterone activates NADPH oxidase,[11,12] suggesting that local aldosterone production in the vascular wall contributes to the generation of ROS and to the subsequent formation of atherosclerotic lesions; however, it has not been investigated whether mechanical stretch influences the production and effect of aldosterone in VSMCs.

Thus, in this study, we investigated the effect of cyclic stretch (CS) on aldosterone synthesis and NADPH oxidase activity in VSMCs. We also tested the effect of eplerenone, a new selective MR antagonist, alone or in combination with Ang II receptor blockers (ARBs), on the CS-induced activation of NADPH.

METHODS

Chemicals

Eplerenone, olmesartan and valsartan were kindly supplied by Pfizer Inc. (New York, NY, USA), Sankyo Co. (Tokyo, Japan) and Novartis Pharma KK (Basel, Switzerland), respectively. Spironolactone, SB203580 and 11-deoxycorticosterone acetate were purchased from Sigma-Aldrich (St Louis, MO, USA). U0126 was purchased from Cell Signaling Technology (Beverly, MA, USA). SP600125 was purchased from Biomol Research Laboratories (Plymouth, PA, USA).

Cell culture

The investigation conforms with the Guide for the Care and Use of Laboratory Animals published by the US National Institutes of Health (NIH publication no. 85-23, revised 1996). Rat aortic smooth muscle cells (RASMCs) isolated from the thoracic aorta of male Sprague–Dawley rats by explants were maintained in growth medium (Dulbecco's modified Eagle's medium (1000 mg glucose/l) (Sigma-Aldrich) containing 10% fetal bovine serum (Life Technologies, Gaithersburg, MD, USA), 100 U ml^{-1} penicillin G and 0.1 μg ml^{-1} streptomycin). RASMCs between passages 3 and 10 were used for experiments after 24 h of serum starvation.

CS apparatus

RASMCs (1×10^6) were seeded in a silicon chamber (32 mm length, 32 mm width and 10 mm depth) pre-coated with 50 μg ml^{-1} bovine plasma fibronectin (Sigma-Aldrich). RASMCs were incubated with growth medium for 24 h and, thereafter, the medium was replaced with starvation medium (Dulbecco's modified Eagle's medium containing 0.1% bovine serum albumin). After serum deprivation for 24 h, the medium was again replaced with fresh starvation medium and the cells were exposed to uniaxial CS (5–20% elongation, 0.5 Hz) using NS-750 (Strex, Osaka, Japan), as previously described,[13] at 37 °C in a humidified atmosphere of 95% air/5% CO_2. Control RASMCs (static control) were starved in the same manner as CS cells and were placed in fresh starvation medium before being maintained in an incubator.

Measurement of NADPH oxidase activity

NADPH oxidase activity was measured by determining the chemiluminescence of lucigenin (5 μmol l^{-1}; Sigma) as previously described,[14] with minor modifications. Briefly, cells were lysed by sonication and centrifuged for 10 min at 8000 *g*. The supernatant was further centrifuged for 1 h at 100 000 *g*. The pellet was used as the membrane fraction. The membrane protein (10 μg) was resuspended in a balanced salt solution of the following composition (mmol l^{-1}): NaCl, 128; KCl, 2.5; $MgSO_4$, 1.0; $CaCl_2$, 2.7; HEPES, 20; glucose, 16; pH 7.4. To prevent nonspecific chemiluminescence, 5 μl of EGTA (100 mmol l^{-1}) and 5 μl of NaN_3 (100 mmol l^{-1}) were added; 5 μl of flavin adenine dinucleotide (1 mmol l^{-1}) was also added as a substrate, and then 50 μl of lucigenin (50 μmol l^{-1}) was added to the cell suspension and incubated at 37 °C for 5 min in the dark. Immediately after 25 μl of β-NADPH (10 mmol l^{-1}) was added, chemiluminescence was measured using a Luminometer (LB9507, Berthold, Bad Wildbad, Germany). Superoxide dismutase (50 U) (Sigma) was added to stop superoxide production.

Reverse-transcription PCR

Total cellular RNA was extracted with TRIzol Reagent (Invitrogen, Carlsbad, CA, USA). Reverse-transcription PCR was performed using Ready-To-Go RT-PCR beads (Amersham–Pharmacia Biotech, Piscataway, NJ, USA) as previously described.[15] On the basis of the GenBank database, the PCR primers were used as follows: p22, 5′-CATTGCCAGTGTGATCTACC-3′ and 5′-ATTACAGTGGGCATCACC-3′; Nox1, 5′-GGTCAAACAGAGGAGAGCATGA-3′ and 5′-CCAGCACAGCCACTTCATAC-3′; Nox2, 5′-GCTGTTCAATGCTTGTGGCT-3′ and 5′-TCTCCTCATCATGGTGCACA-3′; Nox4, 5′-ATTTTCTCAGGCGTGCATGTGG-3′ and 5′-GGAAATGAGCTTGGAACTTGGG-3′; $p47^{phox}$, 5′-TACTTCAACAGCCTCATGGGAC-3′ and 5′-AGTAGCCTGTGACGTCGTCT-3′; $p67^{phox}$,5′-CCACTCGAGGATTTGCTTCA-3′ and 5′-ATCTTGGAATGCCTGGGCTC-3′; NOXO1, 5′-GCCTGCTACGGAGATCTGA-3′ and 5′-TTCTCCACCAGCCACCAGCCT-3′; NOXA1, 5′-CACGGTCATCAAAGTTCTAGCC-3′ and 5′-GGAGACTTGAGACAGTAGT-3′ and GAPDH, 5′-CGGAGTCAACGGATTTGGTCGTAT-3′ and 5′-AGCCTTCTCCATGGTGGTGAAGAC-3′. Primers for CYP11B2, 11β-HSD2 and MR were designed as previously described.[16,17] Cycle numbers were 35 for Nox2, $p47^{phox}$, $p67^{phox}$, NOXO1, NOXA1 and MR, 30 for Nox1, CYP11B2 and 11β-HSD2, 28 for Nox4 and 24 for GAPDH. Each mRNA level was normalized to that of GAPDH and is given as the fold increase against the basal values.

Western blotting

Cells were harvested with a Laemmli sample buffer containing 100 mmol l^{-1} dithiothreitol. Total lysate was sonicated and boiled, and thereafter samples (10 μg per lane) were separated by SDS-PAGE with a 10% polyacrylamide gel and transferred to a nitrocellulose membrane using a Trans-Blot SD Semi-Dry Transfer Cell (Bio-Rad, Richmond, CA, USA). After blocking with 5% skim milk for 1 h, the membrane was probed with a primary antibody. Polyclonal antibodies for phosho-ERK1/2 (Cell Signaling Technology), ERK1/2 (Cell Signaling Technology), phosho-JNK1/2 (Cell Signaling Technology), JNK1/2 (Upstate Biotechnology Inc., Lake Placid, NY, USA) and p38 (Santa Cruz Biotechnology Inc., Santa Cruz, CA, USA), and monoclonal antibodies for phosho-p38 (Santa Cruz Biotechnology Inc.) and CYP11B2 (Chemicon, Temecula, CA, USA) and β-actin (Calbiochem, La Jolla, CA, USA) were used. The membrane was washed three times and incubated with horseradish peroxidase-conjugated anti-rabbit IgG (Cell Signaling Technology) or anti-mouse IgG (Cell Signaling Technology) for 1 h. Immunoreactive proteins on the membrane were visualized by treatment with a detection reagent (Lumi-GLO; Cell Signaling Technology). An optical densitometric scan was performed using Science Lab 99 Image Gauge Software (Fuji Photo Film, Tokyo, Japan).

Measurement of aldosterone concentration

Aldosterone concentrations were measured using an enzyme immunoassay kit (Cayman Chemical Corp., Ann Arbor, MI, USA). After cells were exposed to CS or cultured in static conditions, the culture medium was collected. Cells were collected by scraper and sonicated. The culture medium (50 μl) and cellular sample (1×10^6 cells per 50 μl) were diluted with enzyme immunoassay buffer (450 μl) and used directly in the assay according to the manufacturer's instructions.

Cell proliferation assay

To assess RASMC proliferation, we used the BrdU Cell Proliferation Assay (Exalpha Biologicals Inc., Watertown, MA, USA) according to the manufacturer's protocol. RASMCs were cultured in static condition or were exposed to CS (10%, 0.5 Hz) in the absence or presence of eplerenone (10 mmol l^{-1}) for 6 h, and thereafter the cells were incubated overnight in culture medium containing 5-bromo-2-deoxyuridine (2 ml ml^{-1}). The uptake of 5-bromo-2-deoxyuridine was determined with a spectrophotometer (Bio-Tek Instruments, Highland Park, VT, USA) and normalized to the amount of cellular protein, which was measured in parallel samples according to the method of Lowry.

Statistics

Data are expressed as the mean ± s.d. for three or four independent experiments. Statistical significance among groups was assessed with one-way or two-way analysis of variance. When a significant difference was observed in analysis of variance, the difference between two groups was analyzed by appropriate *post hoc* analysis.

RESULTS

CS increased NADPH oxidase activity and Nox1 mRNA expression

First, we examined whether uniaxial CS stimulates NADPH oxidase activity in VSMCs as reported in previous papers.[3,6] CS (0.5 Hz) strength-dependently increased NADPH oxidase activity in RASMCs 2 h after stimulation, although 5% extension did not influence it (Figure 1a). An extension of more than 20% impaired cell adhesion and therefore the activity could not be measured. We also examined the effect of CS (10%, 0.5 Hz) on the mRNA expression of NADPH oxidase subunits, that is membrane components Nox1, Nox2, Nox4 and $p22^{phox}$, and cytosol components $p47^{phox}$ and $p67^{phox}$, and their homologs Nox organizer 1 (NOXO1) and Nox activator 1 (NOXA1). In non-stimulated RASMCs, Nox1, Nox4, $p22^{phox}$ and NOXA1 were clearly detected, although the expression of Nox2, $p67^{phox}$ and NOXO1 was undetectable, and the level of $p47^{phox}$ was very low. CS (10%, 0.5 Hz) significantly increased the mRNA expression of Nox1, whereas that of the other subunits was unaffected (Figure 1b).

CS increased the expression of CYP11B2 and aldosterone production

To test whether CS influences the production of aldosterone in VSMCs, we examined the effect of CS on the expression of CYP11B2, 11β-HSD2 and MR, which contribute to the production or effect of aldosterone. CS (10%, 0.5 Hz) significantly increased the CYP11B2 mRNA expression 30 min after stimulation (Figure 2a), whereas it did not alter the levels of 11β-HSD2 and MR. CS (10%, 0.5 Hz) also significantly increased the CYP11B2 protein level; however, the expression level was much lower (11.7 times) in static RASMCs than in the adrenal gland (Figure 2b). This effect was dependent on the strength of the stretch, with a maximal effect being obtained at 15% (Figure 2c).

To further examine whether CS actually stimulates aldosterone production, we measured the concentration of aldosterone by enzyme immunoassay. Aldosterone concentrations in CS-exposed cells and cell culture medium were below the detected level; however, when measured in the presence of 11-deoxycorticosterone, an aldosterone substrate for CYP11B2, a marked increase in the concentration of aldosterone was observed in the cells (Figure 2d), although aldosterone was still undetectable in the culture medium (data not shown). However, when RASMCs were cultured with a mixture of culture medium and cell lysate obtained from CS-stimulated cells, NADPH oxidase activity was significantly increased when compared with cells cultured with those from static conditioned cells (Figure 2e).

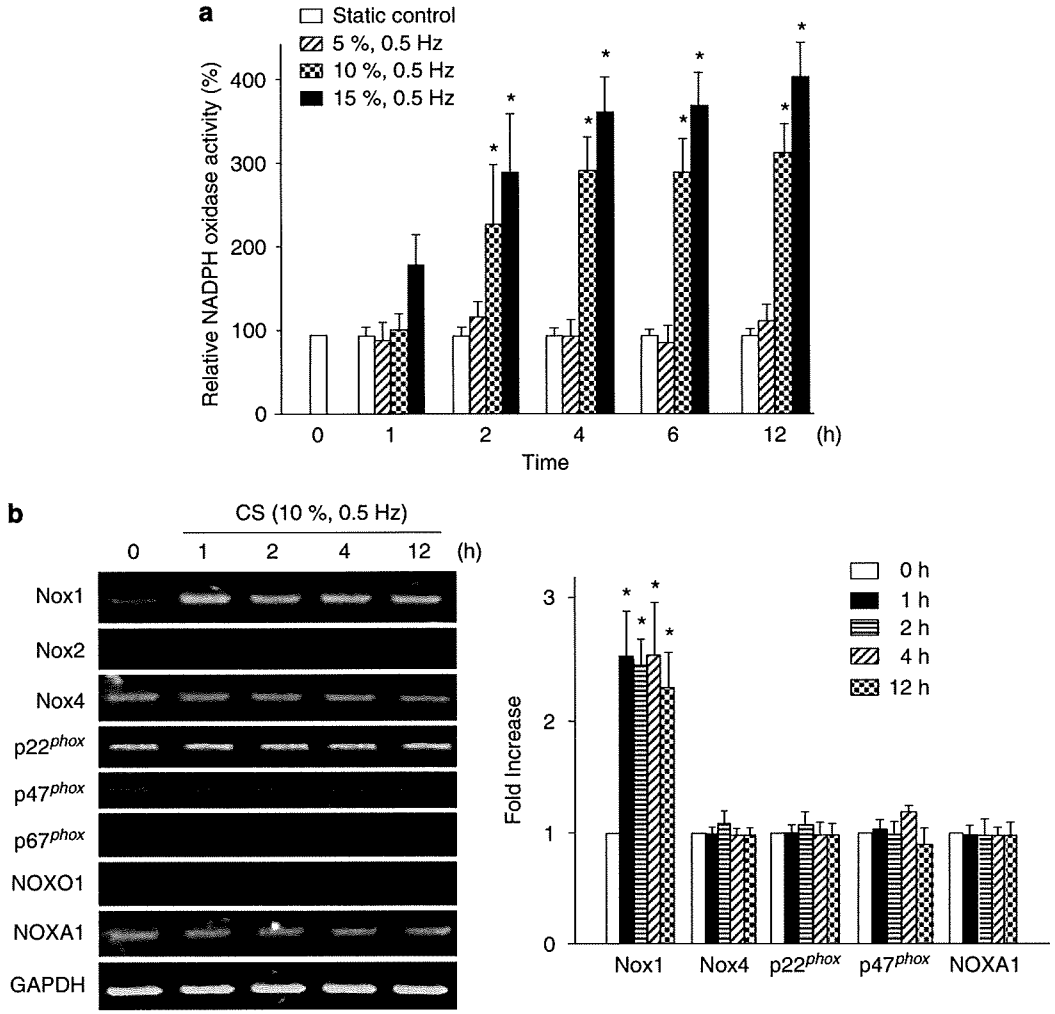

Figure 1 (**a**) Effect of cyclic stretch (CS) on nicotinamide adenine dinucleotide phosphate (NADPH) oxidase activity. Rat aortic smooth muscle cells (RASMCs) were exposed to CS of various strengths (0.5 Hz) for the periods indicated. NADPH oxidase activity is given as the fold increase over the value obtained at time 0. *$P<0.01$ *vs.* static control at each time. (**b**) Effect of CS on the expression of NADPH oxidase subunits. RASMCs were exposed to CS (10%, 0.5 Hz) for the periods indicated. The normalized mRNA expression of NADPH oxidase subunits is given as the fold increase over the value obtained at time 0. *$P<0.01$ *vs.* time 0.

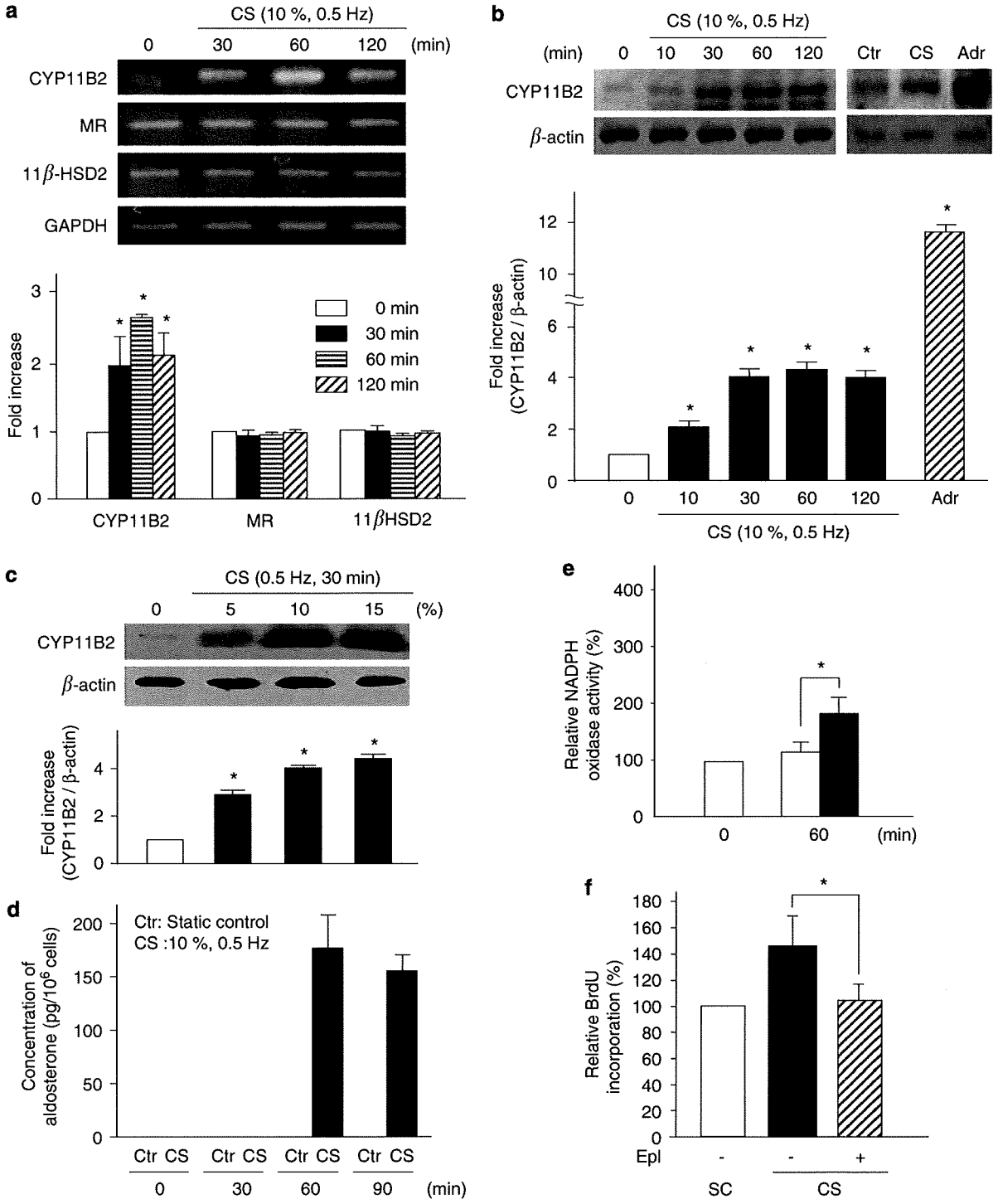

Figure 2 (**a**) Effects of CS on the mRNA expressions of aldosterone-related proteins. Rat aortic smooth muscle cells (RASMCs) were exposed to cyclic stretch (CS) (10%, 0.5 Hz) for the periods indicated. The normalized mRNA level is given as the fold increase over the value obtained at time 0. *$P<0.01$ *vs.* time 0. (**b**) Effect of CS on the expressions of CYP11B2 protein. Left upper panel: RASMCs were exposed to CS (10%, 0.5 Hz) for the periods indicated. Right upper panel: RASMCs were cultured in static conditions (Ctr) or exposed to CS (10%, 0.5 Hz) for 60 min. Adrenal gland (Adr) was obtained from Sprague–Dawley rats. The normalized expression of CYP11B2 protein is given as the fold increase over the value obtained at time 0. *$P<0.01$ *vs.* time 0. (**c**) Strength dependency of the induction of CYP11B2 by CS. RASMCs were exposed to the indicated strengths of CS for 30 min. *$P<0.01$ *vs.* 0%. (**d**) Secretion of aldosterone by CS in the presence of substrate. RASMCs were cultured in static conditions (Ctr) or exposed to CS (10%, 0.5 Hz) in the presence of 11-deoxycorticosterone for the periods indicated. The aldosterone concentration in cells was determined as described in Methods and was shown as pg per 10^6 cells. (**e**) Activation of nicotinamide adenine dinucleotide phosphate (NADPH) oxidase by a mixture of culture medium and cell lysate obtained from CS-stimulated cells. RASMCs were cultured at the indicated times in mixtures of cultured medium and cell lysates obtained from static cells (open bar) or CS-stimulated cells (closed bar), respectively. NADPH oxidase activity is given as the fold increase over the value obtained at time 0. *$P<0.01$. (**f**) Effects of eplerenone on CS-induced increase in DNA synthesis. After serum starvation for 24 h, RASMCs were immediately exposed to CS (10%, 0.5 Hz) for 6 h in the absence or presence of Epl (10 μmol l^{-1}) and thereafter incubated with 5-bromo-2-deoxyuridine (BrdU). BrdU incorporation was measured and analyzed as described in Methods. The data are presented as values relative to the static control (SC) in the bar graph. *$P<0.05$.

As aldosterone exerts its hormonal effects through binding to MR, we subsequently examined whether antagonizing MR is able to suppress CS-induced cellular responses. As shown in Figure 2f, exposure to CS for 6 h significantly increased RASMC proliferation evaluated by 5-bromo-2-deoxyuridine incorporation compared with control (static) cells and, furthermore, a selective MR antagonist, eplerenone (10 μmol l^{-1}), significantly suppressed CS-induced cell proliferation. These results indicate the possibility that a very small amount of aldosterone induced by CS stimulates NADPH oxidase activation and subsequent cellular responses in RASMCs.

Involvement of ERK in CS-induced CYP11B2 expression

The above results suggest that CS stimulates aldosterone synthesis by inducing CYP11B2 expression in RASMCs. Several recent reports have suggested that mitogen-activated protein kinases (MAPKs), such as extracellular signal-regulated kinase (ERK), c-Jun N-terminal

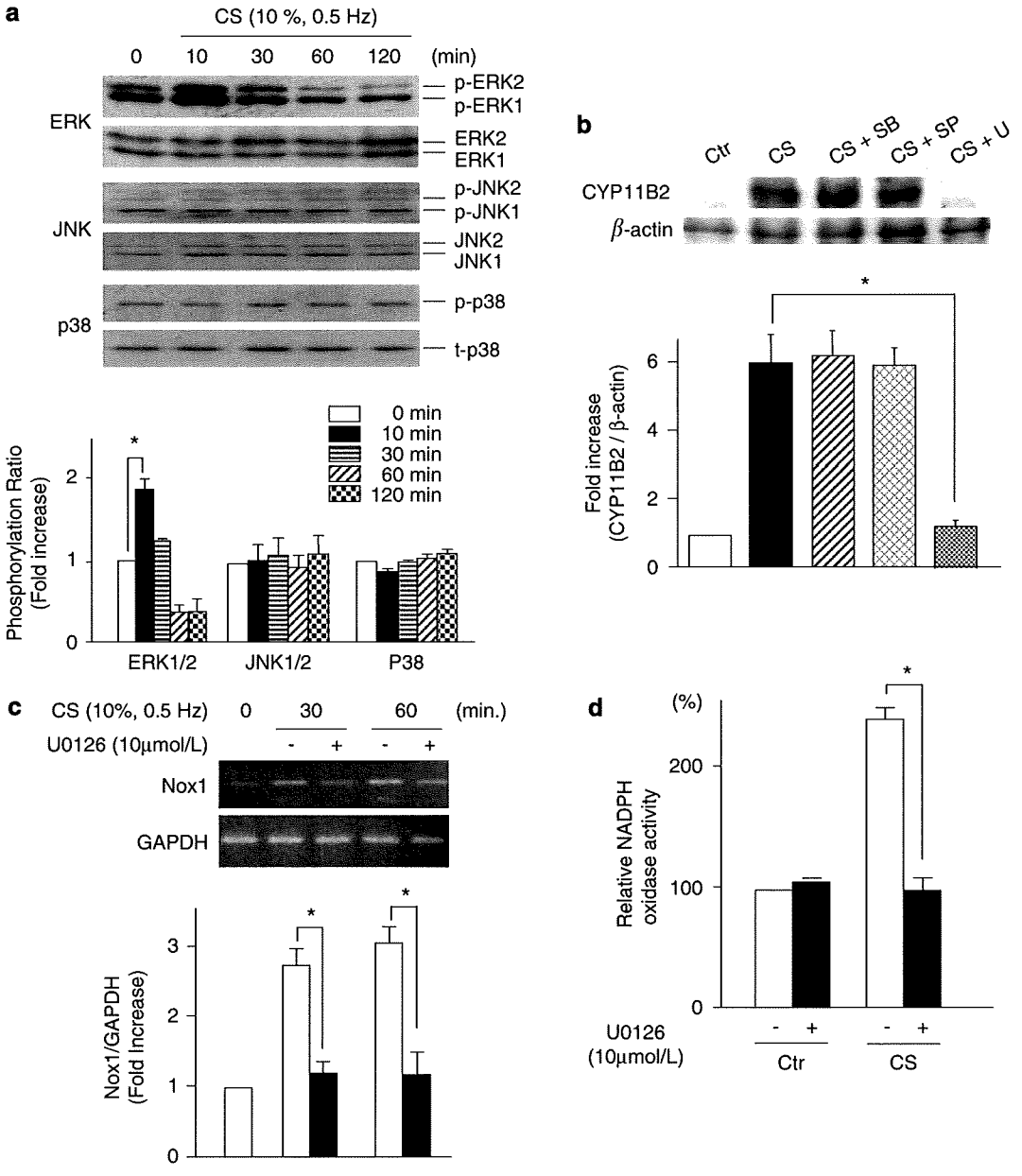

Figure 3 (**a**) Effect of cyclic stretch (CS) on the phosphorylation of mitogen-activated protein kinases (MAPKs). Rat aortic smooth muscle cells (RASMCs) were exposed to CS (10%, 0.5 Hz) for the periods indicated. The phosphorylation ratio of MAPKs is shown as the fold increase over the value obtained at time 0. *$P<0.01$. (**b**) Effect of MAPK inhibitors on CS-induced CYP11B2 expression. RASMCs were exposed to CS (10%, 0.5 Hz) for 30 min with 0.1% dimethyl sulfoxide (CS), 10 μmol l^{-1} of the p38 inhibitor SB203580 (CS+SB), 10 μmol l^{-1} of the JNK inhibitor SP600125 (CS+SP) and 10 μmol l^{-1} of the ERK inhibitor U0126 (CS+U). Control cells (Ctr) were placed under static conditions in an incubator for 30 min. The normalized protein expression of CYP11B2 is given as the fold increase over the value obtained from Ctr. *$P<0.01$. (**c**) Effect of U0126 on the expression of CS-induced Nox1 mRNA. RASMCs were exposed to CS (10%, 0.5 Hz) in the presence or absence of U0126 (10 μmol l^{-1}) for the periods indicated. The normalized mRNA level of Nox1 is given as the fold increase over the value obtained at time 0. *$P<0.01$. (**d**) Effect of U0126 on CS-induced nicotinamide adenine dinucleotide phosphate (NADPH) oxidase activity. RASMCs were exposed to CS (10%, 0.5 Hz) for 2 h in the presence or absence of U0126. NADPH oxidase activity is shown as the fold increase over the value obtained from the static control (Ctr) without U0126. *$P<0.01$.

kinase (JNK) and p38, are activated by CS in VSMCs[18–20] and also contribute to CYP11B2 expression.[21,22] Therefore, we subsequently investigated whether MAPKs are involved in CS-induced CYP11B2 expression. CS (10%, 0.5 Hz) transiently activated ERK; however, the activation of JNK and p38 was not altered (Figure 3a). Pre-treatment with the ERK1/2 inhibitor, U0126, almost completely suppressed CS-induced CYP11B2 expression (Figure 3b), whereas, by contrast, a p38 inhibitor, SB203580, and a JNK1/2 inhibitor, SP600125, did not affect the expression. U0126 also suppressed the CS-induced expression of Nox1 (Figure 3c) and NADPH oxidase activity (Figure 3d), suggesting that ERK has a key role in the expression of CYP11B2 induced by CS.

Aldosterone increased NADPH oxidase activity

To confirm the effect of aldosterone on NADPH oxidase activity, RASMCs were treated with exogenous aldosterone (100 nmol l^{-1}). Aldosterone significantly increased both Nox1 mRNA expression and NADPH oxidase activity (Figures 4a and b). We subsequently examined whether antagonizing MR is able to suppress aldosterone-induced NADPH oxidase activity. When we treated RASMCs with eplerenone (10 μmol l^{-1}), aldosterone-induced increases in Nox 1 expression and NADPH oxidase activity were strongly suppressed (Figures 4c and d), suggesting that aldosterone stimulates NADPH oxidase activity mainly through MR. By contrast, eplerenone did not affect the CS-induced CYP11B2 expression and ERK phosphorylation (data not shown).

ARB inhibited CS-induced CYP11B2 expression and NADPH oxidase activity

Ang II is a major stimulator of aldosterone synthesis that has also been reported to have an important role in NADPH oxidase activity. To determine whether Ang II is involved in the CS-mediated production of aldosterone and activation of NADPH oxidase, we examined the effect of an ARB, olmesartan. Ang II (100 nmol l^{-1}) increased the ERK phosphorylation (Figure 5a) and Nox 1 expression (Figure 5b) in RASMCs. Ang II also induced CYP11B2 expression, although the effect was relatively small (Figure 5c). U0126 almost completely suppressed the Ang II-induced expression of Nox 1 and CYP11B2 (Figures 5b and c).

In RASMCs exposed to Ang II, olmesartan at concentrations of 10 nmol l^{-1} and above almost completely suppressed Ang II-stimulated NADPH oxidase activity (Figure 5d). Pre-treatment with 100 nmol l^{-1} of olmesartan significantly, but not completely, suppressed CS-induced CYP11B2 expression (Figure 5e). As shown in Figure 5f, olmesartan significantly but not completely suppressed the CS-induced ERK1/2 phosphorylation, suggesting that CS-induced CYP11B2 expression through the activation of ERK is partially dependent on Ang II, although other Ang II-independent pathways may also exist.

Additive effects of aldosterone on Ang II-induced ERK phosphorylation, Nox1 expression and NADPH oxidase activity

We further examined whether aldosterone has additive effects on ERK phosphorylation, Nox1 expression and NADPH oxidase activity when

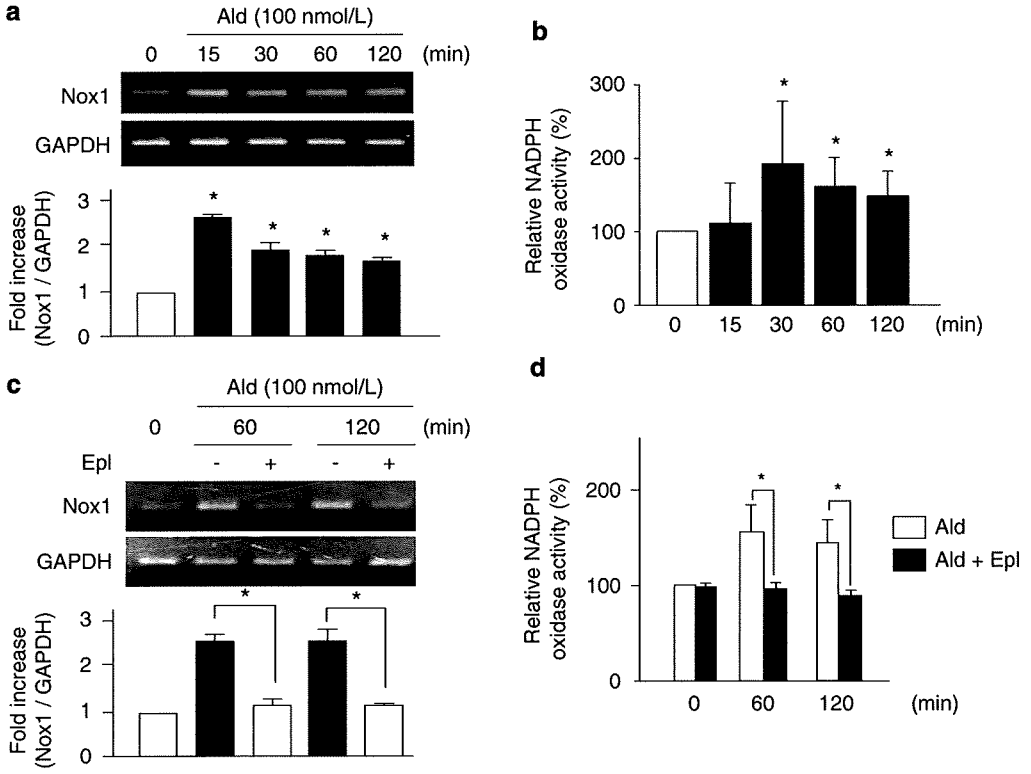

Figure 4 (**a**) Effect of aldosterone on the expression of Nox1 mRNA. Rat aortic smooth muscle cells (RASMCs) were treated with 100 nmol l^{-1} aldosterone (Ald) at the indicated times. The normalized mRNA level of Nox1 is given as the fold increase over the value obtained at time 0. *$P<0.01$ *vs.* time 0. (**b**) Effect of aldosterone on the nicotinamide adenine dinucleotide phosphate (NADPH) oxidase activity. RASMCs were treated as described in (**a**). NADPH oxidase activity is presented as the fold increase over the value obtained at time 0. *$P<0.01$ *vs.* time 0. (**c**) Effect of eplerenone (Epl) on Ald-induced Nox1 expression. RASMCs were stimulated with Ald (100 nmol l^{-1}) in the absence or presence of Epl (20 μmol l^{-1}) for the periods indicated. The normalized mRNA level of Nox1 is given as the fold increase over the value obtained at time 0. *$P<0.01$ *vs.* time 0. (**d**) Effect of Epl- on Ald-induced NADPH oxidase activity. RASMCs were treated as described in (**c**). NADPH oxidase activity is presented as the fold increase over the value obtained at time 0. *$P<0.01$.

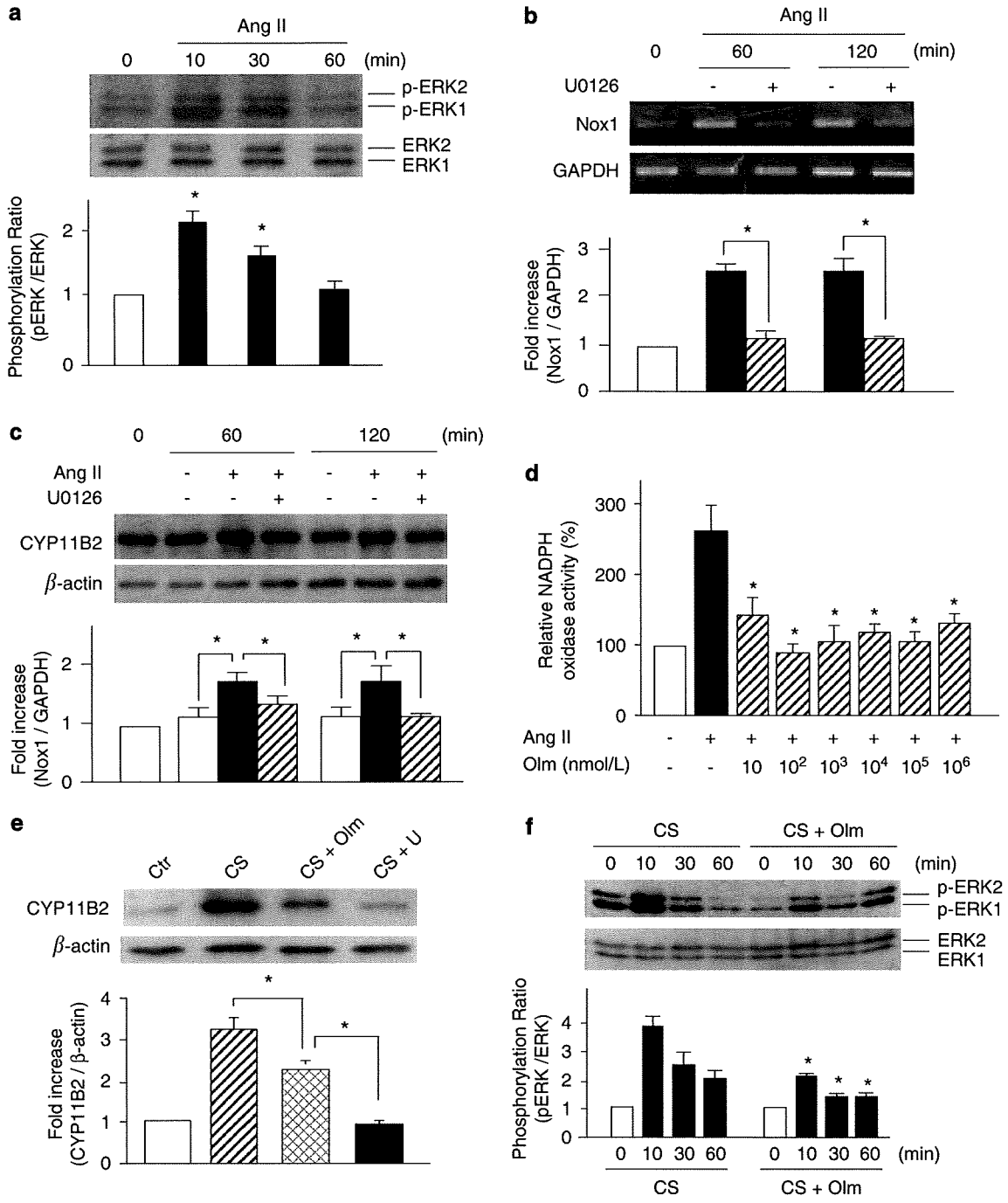

Figure 5 (**a**) Effect of angiotensin II (Ang II) (100 nmol l^{-1}) on ERK1/2 phosphorylation. The phosphorylation ratio is shown as described in Figure 3a. *$P<0.01$ *vs.* time 0. (**b**) Effect of U0126 on Ang II-induced Nox1 expression. Rat aortic smooth muscle cells (RASMCs) were stimulated with Ang II (100 nmol l^{-1}) in the presence or absence of U0126 (10 μmol l^{-1}). The normalized expression of Nox1 mRNA is presented as the fold increase over the value obtained at time 0. *$P<0.01$. (**c**) Effect of U0126 on Ang II-induced CYP11B2 expression. RASMCs were treated as described in (**b**). The normalized expression of CYP11B2 is presented as the fold increase over the value obtained at time 0. *$P<0.05$. (**d**) Effect of olmesartan (Olm) on Ang II-induced nicotinamide adenine dinucleotide phosphate (NADPH) oxidase activity. RASMCs were stimulated with Ang II (100 nmol l^{-1}) in the presence of the indicated concentrations of Olm. NADPH oxidase activity is presented as the fold increase over the value obtained from static control cells (open bar). *$P<0.01$ *vs.* Ang II-stimulated cells without Olm (closed bar). (**e**) Effect of Olm on cyclic stretch (CS)-induced CYP11B2 expression. RASMCs were exposed to CS (10%, 0.5 Hz) in the presence of 100 nmol l^{-1} of Olm (CS+Olm) or 10 μmol l^{-1} of U0126 (CS+U). The normalized CYP11B2 expression is given as the fold increase over the value obtained from static control cells (Ctr). *$P<0.01$. (**f**) Effect of olmesartan (Olm) on CS-induced ERK phosphorylation. RASMCs were exposed to CS (10%, 0.5 Hz) in the absence or presence of Olm (100 nmol l^{-1}) for the periods indicated. The phosphorylation ratio is shown as described in Figure 3a. *$P<0.01$ *vs.* CS at each time.